CHALMERS

A stability Analysis of the Active Thermal Control System of the Columbus space laboratory

Master of Science Thesis

TOR KLINGBERG

Department of Signals and Systems
Division of Automatic Control, Automation and Mechatronic
CHALMERS UNIVERSITY OF TECHNOLOGY
Göteborg, Sweden, 2011
Report No. EX010/2011

A stability Analysis of the Active Thermal Control System of the Columbus space laboratory

TOR KLINGBERG

Summary
An analysis has been done on the stability properties of the Automatic Thermal Control System of the European Columbus module of the International Space Station. The study uses the simplified Nyquist stability criterion from classical control theory to determine the stability of a simplified model of the system. Stability margins are calculated for various configurations. The results are compared with transient simulations.

Sammanfattning
En analys har gjorts av stabilitetsegenskaperna för det automatiska temperaturkontrollsystemet i den europeiska Columbus-modulen på den internationella rymdstationen ISS. Studien använder Nyquists förenklade stabilitetskriterium från klassik reglerteori för att avgöra stabiliteten hos en förenklad modell av systemet. Stabilitetsmarginaler beräknas för olika konfigurationer. Resultaten jämförs med transientsimuleringar.

This is a master’s thesis at the department of Signals and Systems, division of Automatic Control, Automation and Mechatronics, Chalmers University of Technology, Sweden. The examiner is professor Claes Breitholtz.
The work was performed at the European Space Research and Technology Centre (ESTEC) in Noordwijk, the Netherlands.

Contents

Chapter 1—Introduction

Background

The Columbus module is a science laboratory that is part of the International Space Station. It is owned by the European Space Agency and was launched on February 7, 2008 aboard Space Shuttle Atlantis. The module has a water loop cooling system that collects waste heat from the air, the payload racks and the modules subsystems such as power converters. The heat is transported to heat exchangers and further by the main ISS ammonia cooling system to radiators on the truss. Two pairs of mixing valves are controlled by PID regulators to hold temperature setpoints. The function and stability of the system have been verified by computer simulation and ground tests in various situations. However, no verification using control theory has been conducted; specifically, the stability of the control system has not been analytically verified. A theoretical analysis of the system can help verify that the simulations and tests are accurate, and that they have not missed any instability in the system. Control theory can also give a picture of how changing the control parameters affects the performance and stability of the system.

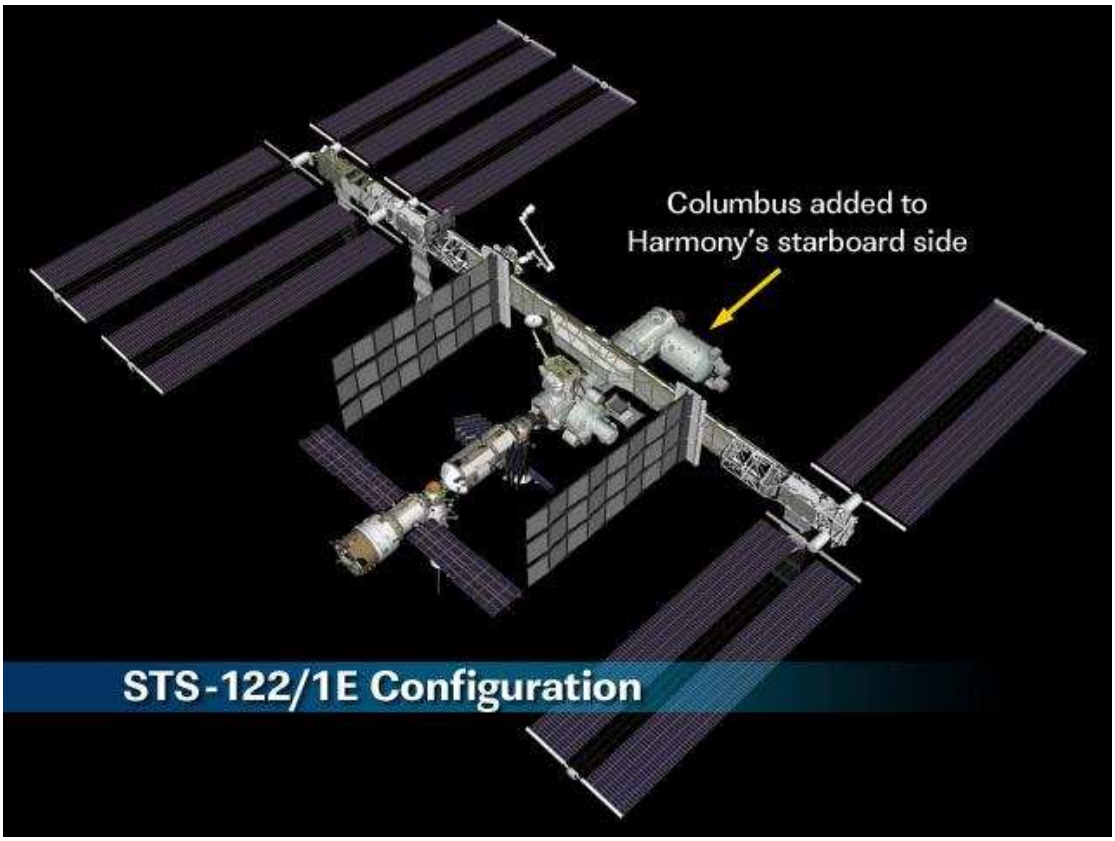

Figure 1: Location of Columbus on the International Space Station. More modules have since been attached.

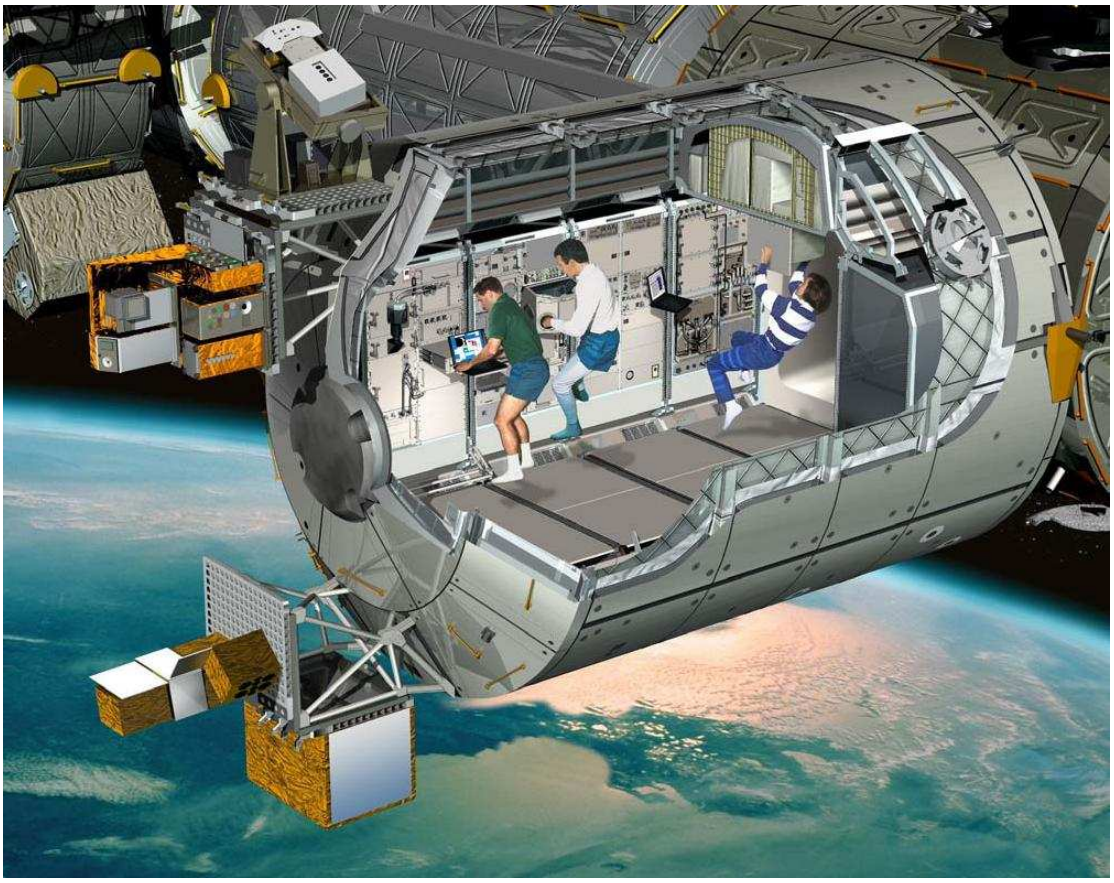

Figure 2: Artist's impression of the Columbus Laboratory, cutaway view. (Image: ESA/Ducros)

Previous work

The performance and stability of the Columbus Active Thermal Control System water loop have been verified by simulation, physical testing on a breadboard setup, and ultimately by tests on the Columbus Proto-Flight Model (PFM).

The simulation was done using the thermal software tool ESATAN/FHTS with a mathematical model of the system. [1][2][3][4][5][6]

This study adopts a similar approach adopted for Node 2 and 3 [7].

Purpose

The purpose of this master's thesis is to improve the understanding of the stability of the Automatic Thermal Control System of the Columbus module of the International Space Station. It aims to confirm simulations and breadboard tests with a theoretical model and to give increased confidence in the reliability of the control system. A study of the control system can also reveal possible flaws or unsafe configurations. It

can provide useful methods and techniques for evaluating future thermal control systems for manned spacecraft.

A further goal is to study the stability properties of the system under circumstances that were not anticipated in the original design of the module. One example is control parameters far from normal values.

Another interesting operating condition is when the water temperature setpoint at the Condensing Heat Exchangers (CHX) are raised from 5 to 10°C. They will then no longer actually condense air humidity into water. This is possible if the condensation takes place in another part of the space station, but is different from what the Columbus Automatic Thermal Control System was made for. Therefore, finding if such a configuration could lead to system instability would be useful.

Control theory basis

In classical control theory, a system including the controller is described as a complex transfer function and its stability is determined by analyzing the properties of the transfer function. To get a transfer function description we start with a differential equation connecting a system input variable u(t) and output variable y(t).[10] For example,

$$\frac{dy(t)}{dt} = (u(t))^2 - y(t)$$

Since this is a non-linear differential equation, it first has to be linearized around a working point $u_0, y_0,\ u_0{}^2 - y_0 = 0$

$$\frac{d(y(t) - y_0)}{dt} = u_0^2 + 2u_0 \cdot (u(t) - u_0) - y_0 - (y(t) - y_0)$$

$$\frac{dy(t)}{dt} = 2u_0 u(t) - u_0^2 - y(t)$$

This linear differential equation can now be Laplace transformed

$$s \cdot Y(s) = 2u_0 \cdot U(s) - Y(s)$$

$$G(s) = \frac{Y(s)}{U(s)} = \frac{2u_0}{s+1}$$

Here $G(s)$ is the transfer function that describes how a small disturbance in input variable u affects the system output y.

When there is a controller, it is typically connected to the system in a feedback loop.

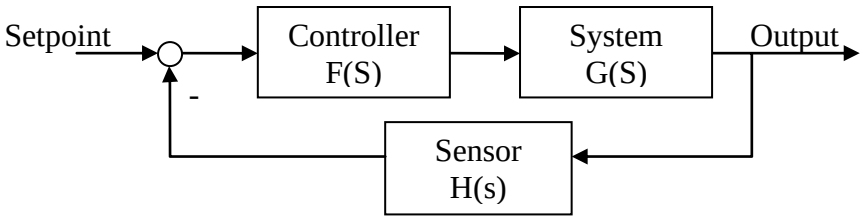

The closed loop transfer function that describes how a small change in the controllers input affects the system output, is

$$K(s) = \frac{G(s)F(s)}{1 + G(s)F(s)H(s)}$$

The mathematical properties of the open loop transfer function gives important information about the stability of the closed loop control system.
See the section Simplified Nyquist Stability Criterion below.

Method outline

First, the system is described and the relevant parts are isolated. It is simplified to allow a theoretical analysis and a mathematical model using differential equations of each relevant parts of the system is constructed. The differential equations are linearized and transformed into transfer functions, and the transfer functions are connected into two combined transfer functions (one for each valve), describing the whole chain from control valve to temperature sensor. A method to measure stability margin using the Nyquist criterion of classical control theory is chosen, and the stability of the system with given parameters is determined. Maps of the stability margin depending on three control parameters are constructed for different working points. Finally the results are compared to numerical transient simulations and the validity of some simplifications is tested.

Chapter 2—System description

The water loop temperature control system supplies the payload racks, subsystems and condensing heat exchangers with cooling water of a regulated temperature and pressure, and transports heat from there and from the cabin air to heat exchangers, where the water is cooled by ammonia. Figure 3 shows the system layout.

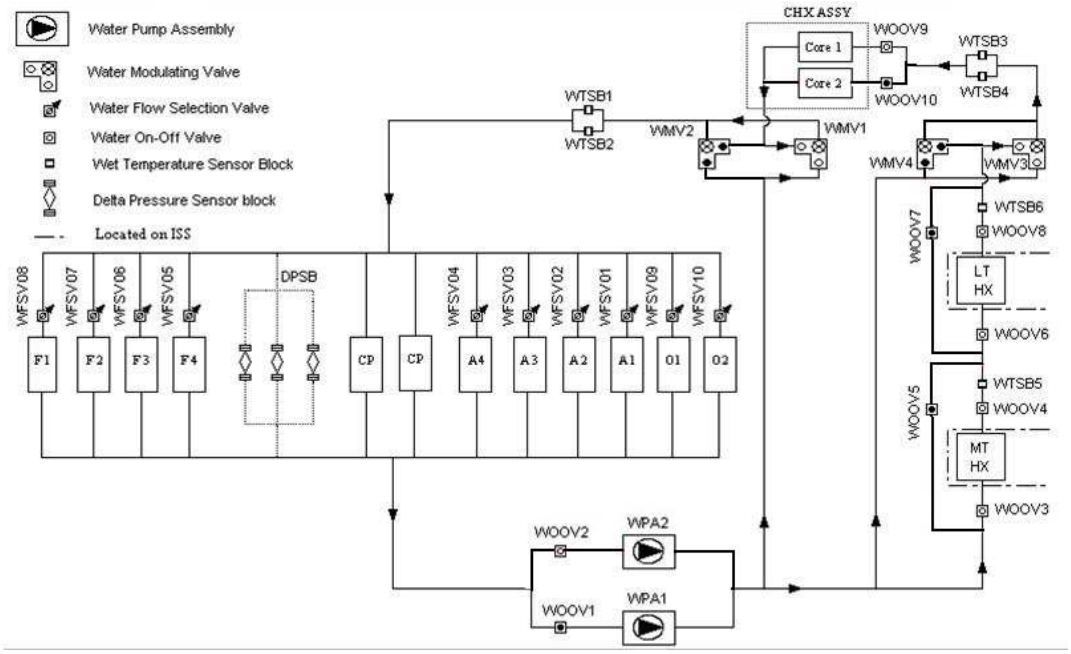

Figure 3 – Automatic Thermal Control System schematic [3]

The system consists of:

- Two Water Pump Assemblies (WPA), one running, one redundant.
- High-temperature (HT) and low-temperature (LT) water/ammonia heat exchangers
- Four Water Modulating Valves (WMV) in two pairs
- Six Wet Temperature Sensor Blocks (WTSB) in two pairs and one after each water/ammonia heat exchanger
- One Condensing Heat Exchanger (CHX) with two core elements
- 10 connectors for International Standard Payload Racks (ISPR), each with a Water Flow Selection Valve (WFSV)
- 24 cold plates for avionics boxes in two series

- Three Delta Pressure Sensor Blocks (DPSB) with two sensors each
- A number of Water On-Off Valves (WOOV)

Starting from the Water Pump Assemblies, the water flows to the water–ammonia heat exchangers, starting with the medium-temperature (MT) HX. It continues to the low-temperature (LT) HX where it is cooled to 3 °C (1.1–6.1 °C). There is bypass piping past each of the MT and LT heat exchangers, but these are closed under normal operation. There is also a bypass past both the heat exchangers. This warm water is mixed with the cold water in Water Modulating Valve (WMV) 3 or 4; one is active and one is redundant with its internal on-off valve closed.

After the valve, the water temperature is measured in Wet Temperature Sensor Blocks (WTSB) 3 and 4. The measured temperature is used by the digital controller to control the valve position to keep the mixed water temperature near the setpoint, currently 5°C. The mixed water flows to the Condensing Heat Exchanger (CHX) and through one of its core elements, cooling the air and condensing the water. The cooling water then continues to WMV 1 or 2 (depending on which in the redundant pair is open), where it is again mixed with warm water from a bypass directly from the pump. The mixed water temperature is measured at WTSB 1 and 2, and used to control the valve position to hold a set point for the plenum inlet, planned at 17 °C.

The plenum consists of payload racks, a cold plate series and Delta Pressure Sensor Blocks (DPSB), all connected in parallel. The pressure drop over the plenum is measured by the DPSBs and held between 40 and 44 kPa by controlling the pump speed. The water flow rate through each payload rack is controlled by a Water Flow Selection Valve (WFSV) and possibly internally in some payloads. After passing through the plenum, the water flows back to the pump.

Controllers

Of particular interest here is the automatic control system. The controllers for the pumps and valves are located at the WPA Electronic Package Controller (EPC). They are Proportional-Integrative-Derivative (PID) controllers implemented digitally with a sampling frequency of 1 Hz. The EPC software also controls the pump inlet pressure by controlling the pressure in an accumulator.

This study is primarily concerned with the thermal control, which is performed using the valves. The output of the controller at time step n is calculated as: [8]

$$X_n = X_{n-1} + (k_p + \frac{k_i \cdot \Delta t}{2} + \frac{k_d}{\Delta t}) \cdot Err_n + (\frac{k_i \cdot \Delta t}{2} - k_p - \frac{2 \cdot k_d}{\Delta t}) \cdot Err_{n-1} + \frac{k_d}{\Delta t} \cdot Err_{n-2}$$

where

Xn = controller output at time step n, change In valve position

Err_n = controller input = set-point value – measured value

= $Y_{sp} - Y$

Err_{n-1} = controller input one time step before

Err_{n-2} = controller input two time steps before

k_p = proportional gain constant

k_i = integrative gain constant

k_d = derivative gain constant

Dt = sampling period (1 s)

The output of the controller is a change in valve position. The valve position α is thus the accumulated (integrated) control signal.

$$\alpha_n = \alpha_{n-1} + X_n$$

This is a discretization of the basic PID control law

$$X(t) = k_p \cdot Err(t) + k_i \cdot \int_0^t Err(t')dt' + k_d \cdot \frac{dErr(t)}{dt}$$

The controller is also disabled if the last three measured errors are all inside the dead band, set to ±0.3°C. This is to avoid unnecessary wear on the valves and their control motors.

System simplification

To make a control theory stability analysis, the system must first be simplified in some ways. To be able to use one-dimensional control theory, it is separated into two parts: one for the temperature control for the CHX inlet, and one for the plenum inlet control. The CHX "right" part consists of the water–ammonia heat exchangers (MT and LT), the HX bypass, WMV3&4, WTSB 3&4 and the CHX (Figure 4). The "left" side covers WMV1&2, WTSB1&2, the plenum, pumps and cold side bypass (Figure 5). In the simplified models, the water coming from the other side of the system is assumed to be at a fixed temperature.

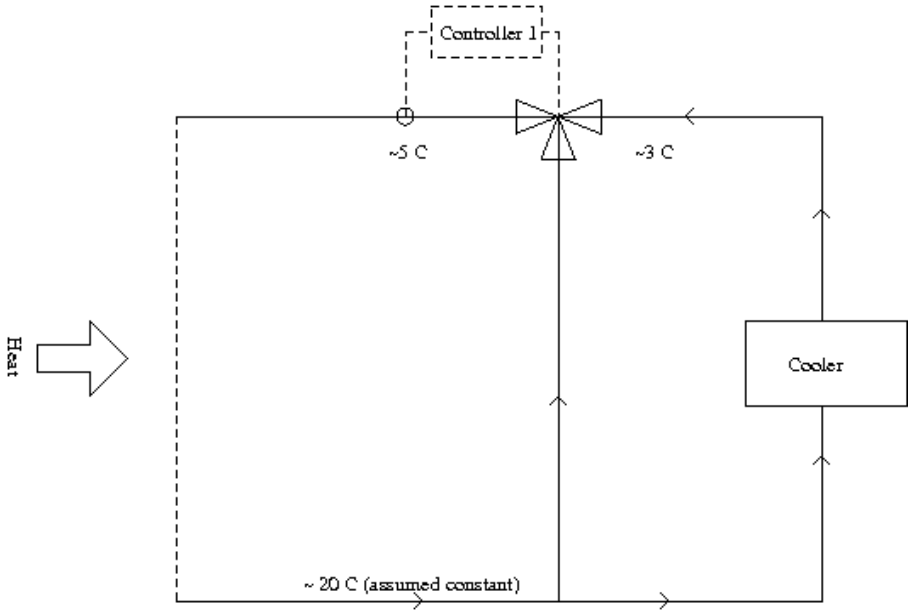

Figure 4 – CHX Inlet subsystem

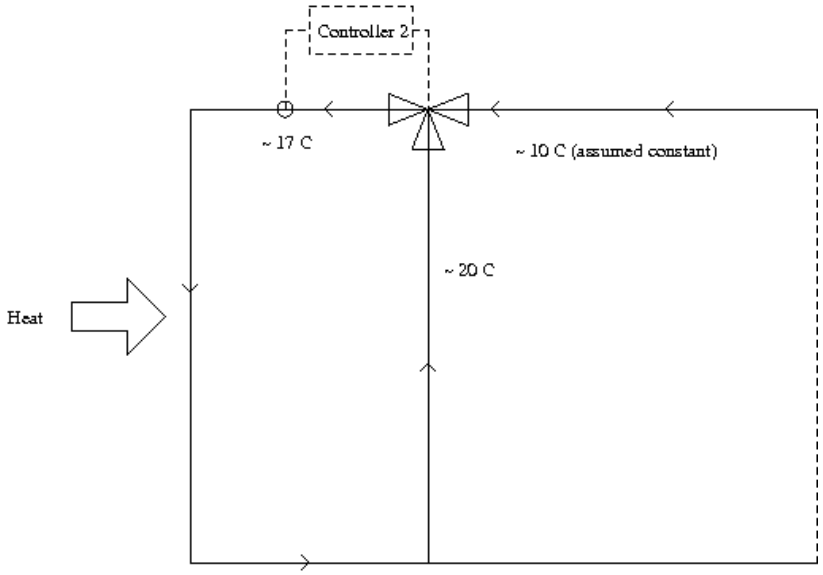

Figure 5 – Plenum inlet subsystem

With the two sides separated, each part is analyzed as a single input – single output (SISO) system, formulating a transfer function description. Specifically, a transfer function that describes how a small change in the system input (signal to the valve control motor) affects the output (temperature measured by the WTSB). That is most easily achieved by combining smaller transfer functions in steps. First, a mathematical model of the system is built, relating valve position, hydraulic resistances, flow rates

and temperatures at various places. Each relation is written in the form of a differential equation.

- Discrete sampling simplified to continuous
- Assumes linear enough

Mathematical model

The mathematical model is based on system descriptions and the Thermal Hydraulic Mathematical Model implemented in ESATAN-FHTS:

CHX INLET SUBSYSTEM MODEL

CHX inlet subsystem model is composed as follows:

WTSB (sensor)

The measured temperature T_s is related to the water temperature at the sensor location T_w by:

$$\tau_s \frac{dT_s(t)}{dt} + T_s(t) = T_w(t)$$

The time constant is related to the rise time of the sensor as

$$\tau_s = \tau_{rise} / 2.2$$

This describes the slowness of the sensor.

WMV (valve)

The water temperature at a valve outlet is determined by the mixing of the cold and hot sides, with temperatures T_{LT} and T_0 respectively, i.e.:

$$\dot{m}_0(t) \cdot T_{out}(t) = \dot{m}_{hx}(t) \cdot T_{LT}(t) + \dot{m}_{by}(t) \cdot T_0(t)$$

With mass flow rates $\dot{m}_{hx}, \dot{m}_{by}, \dot{m}_0$ depending on the hydraulic resistance of the valve and of the upstream branches. Mass rather than volume flow rate is used in the system documentation. The water density is close to constant, so the flow rates easily can be converted when needed.

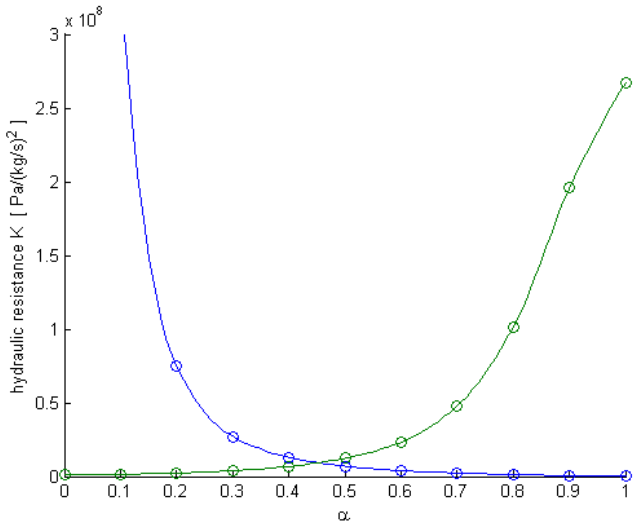

Figure 6 – WMV hydraulic resistance vs valve position

The hydraulic resistance of the two paths in the valve is interpolated from measured data (Figure 6), while the hydraulic resistances of the two branches of piping are computed directly from the pressure drops in the ESATAN-FHTS simulation at the appropriate working point ($dP^{(0)}, \dot{m}^{(0)}$), using Bernoulli's law backwards:

$$K = \frac{dP^{(0)}}{\dot{m}^{(0)2}}$$

Flow rates are then determined by:

$$\dot{m}^2 = \frac{dP}{K}$$

imposing equal pressure drop through the HX and bypass sides

$$dP_{hx} = dP_{by}$$

and mass conservation at the valve outlet

$$\dot{m}_{hx} + \dot{m}_{by} = \dot{m}_0$$

DELAY TIME

Delay times for a temperature change to propagate through piping is calculated as

$$\Delta t = V \cdot \rho / \dot{m}$$

where V is the sum of the volumes of the piping parts placed between the considered elements, and ρ is the density of water. Actually, there is necessarily some mixing in the pipes, which is neglected in this model.

HEAT EXCHANGERS

The effectiveness of the water/ammonia heat exchangers is computed with the classical effectiveness-NTU method [9] for counter flow case:

$$M_{hx} \frac{dT_{hx-out}}{dt} + \dot{m} T_{hx-out} = \varepsilon \dot{m} T_{NH_3} + (1-\varepsilon) \dot{m} T_{hx-in}$$

Where M_{hx} is the water mass in the heat exchanger and the efficiency factor

$$\varepsilon = \dot{m}_{NH3} \frac{\left[1 - \exp\left(-\frac{UA}{C_{P,H2O}}\left(\frac{1}{\dot{m}_{H2O}} - \frac{C_{P,H2O}}{C_{P,NH3}}\frac{1}{\dot{m}_{NH3}}\right)\right)\right]}{\dot{m}_{NH3} - \frac{C_{P,H2O}}{C_{P,NH3}} \cdot \dot{m}_{H2O} \exp\left(-\frac{UA}{C_{P,H2O}}\left(\frac{1}{\dot{m}_{H2O}} - \frac{C_{P,H2O}}{C_{P,NH3}}\frac{1}{\dot{m}_{NH3}}\right)\right)}$$

With the overall conductance UA about 7500 W/°K and a constant ammonia flow rate $\dot{m}_{NH3}$ =930 Kg/h and specific heat of $C_{p,H2O}$=4184 J/Kg/°K and $C_{p,NH3}$=4184 J/Kg/°K.

Chapter 3—Control theory

Linearized system model & transfer functions

Some of the differential equations are non-linear, so they must be linearized around a working point, calculated using an ESATAN/FHTS simulation.

The linearized differential equations are then Laplace transformed to form transfer functions. Actually, since the control system is time-discrete and operates with a finite frequency of 1 Hz, the Z-transform would be more accurate. To use the Laplace transform we have to approximate the controller as a continuous PID regulator. However, since thermal fluctuations are slow compared to 1 Hz, the simplification of the continuous Laplace transform is used.

Components

WMV VALVE

The relation between hydraulic resistances and flow rates past the heat exchangers and though the bypass,

$$\dot{m}_{hx} + \dot{m}_{by} = \dot{m}_0$$

$$dP = K_{hx} \cdot \dot{m}_{hx}^2 = K_{by} \cdot \dot{m}_{by}^2 ,$$

is a quadratic equation that is not easily linearized. It can be solved to

$$\frac{\dot{m}_{hx}}{\dot{m}_0} = -\sigma \pm \sqrt{\sigma^2 + \sigma}, \quad \sigma = \frac{K_{by}}{K_{hx} - K_{by}} \tag{1}$$

Where the sign depends on which gives a physical result $0 \le \frac{\dot{m}_{hx}}{\dot{m}_0} \le 1$

Even though there is a border between the positive and negative square root, it is in fact a continuous function, see Figure 7.

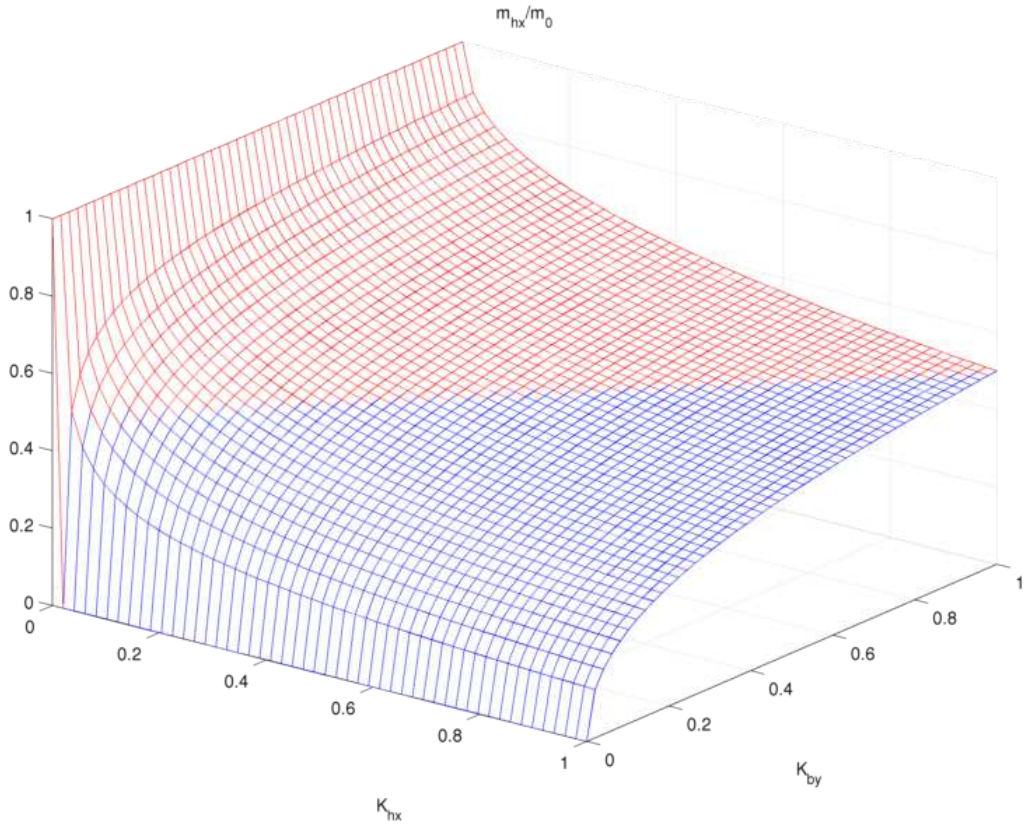

Figure 7 – Flow rate distribution by hydraulic resistances. The blue part is where the root in

$$\frac{\dot{m}_{hx}}{\dot{m}_0} = -\sigma \pm \sqrt{\sigma^2 + \sigma}, \quad \sigma = \frac{K_{by}}{K_{hx} - K_{by}}$$

(1) is positive, red where it is negative.

Still, rather than linearizing this, the values at two valve positions near the working point are compared to calculate the slope.

$$\frac{d\dot{m}_{hx}}{d\alpha} \approx \frac{\dot{m}_{hx}\left(\alpha^0 + \Delta\alpha\right) - \dot{m}_{hx}\left(\alpha^0\right)}{\Delta\alpha},$$

with $\Delta\alpha$ a small value (0.01, compared to the valve opening range of 0–1).

This constant value (for each working point) is used as the transfer function named $AB(s)$

CONTROLLER

The idealized transfer function of the controller is described as

$$PID(s) = k_P + \frac{k_I}{s} + k_D s$$

The derivative term is not physically realizable. The actual controller operation is described on pages 6-7 above. In this approximation the dead band, quantization and the finite sampling frequency of the controller is neglected.

HEAT EXCHANGERS

Here, the following nomenclature is used:

- T_0 - Temperature before the MT heat exchanger. Input temperature.
- T_{hxm} - Temperature after the MT heat exchanger, before the LT heat exchanger.
- T_{hxo} - Temperature after the LT heat exchanger. HX output temperature.
- T_{MT}, T_{LT} - Ammonia temperature in the MT and LT heat exchangers.
- M_{MT}, M_{LT} - Water mass inside the MT and LT heat exchangers.
- λ_{MT}, λ_{LT} - Parameters, used to avoid repeating long definitions.
- ε_{MT}, ε_{LT} - Heat exchanger efficiency factors, per chapter 2 above.

The transfer function describing the flow rate effect on the temperature between the MT and LT heat exchangers is

$$C(s) = \frac{L[T_{hxm}]}{L[d\dot{m}_{hx}]} = \frac{\lambda_{MT}}{M_{MT}s + \dot{m}_{hx}^0}$$

with

$$\lambda_{MT} = (T_{MT} - T_0) \cdot \left(\varepsilon_{MT} + m_{hx} \cdot \frac{d\varepsilon_{MT}}{d\dot{m}_{hx}} \right) + T_0 - T_{hxm}$$

The flow rate effect on the temperature after heat exchangers is

$$F(s) = \frac{L[T_{hxo}]}{L[\dot{m}_{hx}]} = \frac{\lambda_{LT}}{M_{LT}s + \dot{m}_{hx}^0}$$

with

$$\lambda_{LT} = (T_{LT} - T_{hxm}) \cdot \left(\varepsilon_{LT} + m_{hx} \cdot \frac{d\varepsilon_{LT}}{d\dot{m}_{hx}} \right) + T_{hxm} - T_{hxo}$$

The effect of temperature between MT and LT, on the temperature after LT, is:

$$G(s) = \frac{L[T_{hxo}]}{L[T_{hxm}]} = \frac{1 - \varepsilon_{LT}}{M_{LT} / \dot{m}_{hx}^0 \cdot s + 1}$$

VALVES

The direct effect of flow rate on the valve output temperature is

$$I(s) = \frac{T_{hxo}^0 - T_0^0}{\dot{m}_{hx}^0}$$

The effect of HX output temperature on valve output temperature is

$$J(s) = \frac{\dot{m}_{hx}^0}{\dot{m}_0}$$

The last two are constant, but described as transfer functions for consistency.

DELAY TIME

The transfer function for the time delay τ between WMV outlet and temperature sensor is

$$\Delta_\tau(s) = \exp(-s \cdot \tau)$$

SENSOR

Finally, the sensor modeling

$$Sensor(s) = \frac{1}{1 + \tau_s \cdot s}$$

CHX Inlet Subsystem Model

The transfer functions for the CHX inlet side are connected as the following diagram:

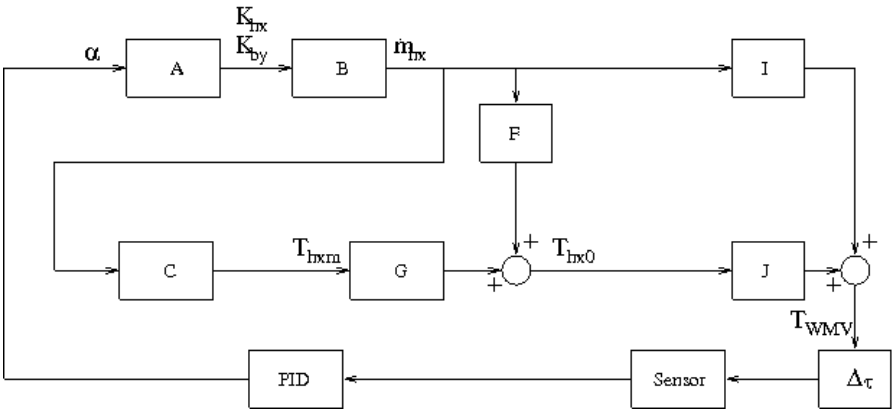

Figure 8 – CHX Inlet subsystem transfer function

By combining transfer functions it can be simplified to:

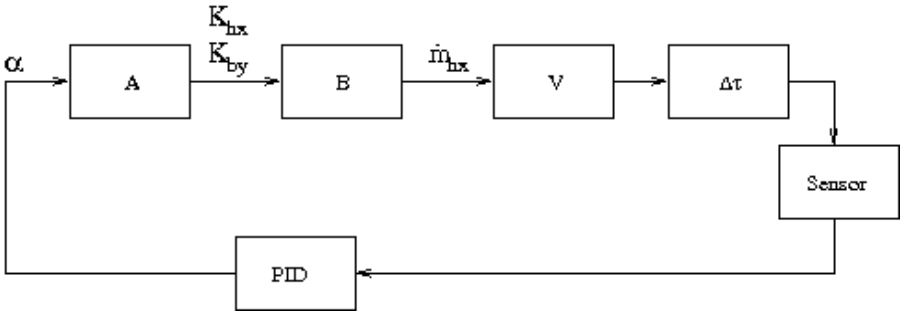

Figure 9 – Simplified CHX inlet subsystem transfer function

where the V block is defined by the transfer function

$$V(s) = I(s) + J(s) \cdot \Delta_{\tau_1}(s) \cdot [F(s) + G(s) \cdot C(s)]$$

Plenum Inlet Subsystem Model

On the plenum side the transfer functions are similar, without the complicated heat exchanger description, but arranged in a different way. One exception is the time for the water to flow through the plenum, pump and back through the cold side bypass to the plenum temperature selection valve. Instead of summing the volumes of all the parts on the way, the time is measured in a transient ESATAN/FHTS simulation by fixing the valve positions, introducing a short heat burst and measuring its travel time. Because of the multiple flow paths through the plenum and the thermal inertia, the

heat wave will be smoothed out on the way. The arrival of the first part of the wave is used to measure travel time. See Figure 10.

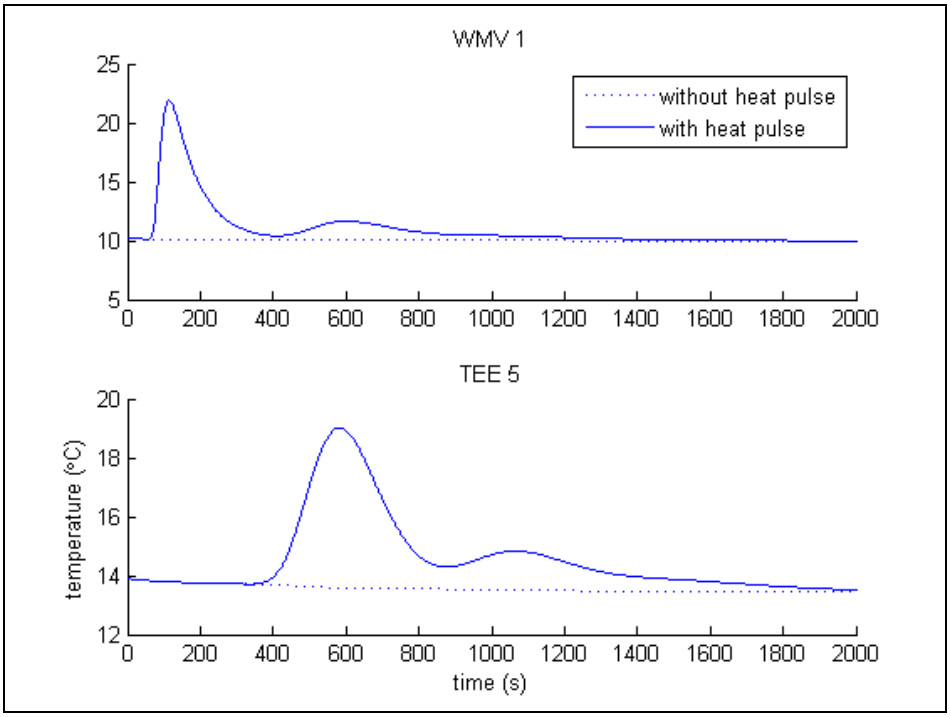

Figure 10 – Heat burst travel time between WMV1 outlet and WMV1 bypass side inlet.

In Figure 11 is reported the transfer function block of the complete subsystem, with the additional transfer functions C^{plenum} and E^{plenum} which describe the plenum behavior:

$$C^{plenum}(s) = \frac{T_{chx} - T_{pump}}{\dot{m}_{hx}}$$

For effect of the flow rate on the temperature after the valve, and

$$E^{plenum}(s) = 1 - \frac{\dot{m}_{hx}}{\dot{m}_0}$$

For the effect of temperature of the water directly from the pump (bypassing the cold side) on temperature after the valve

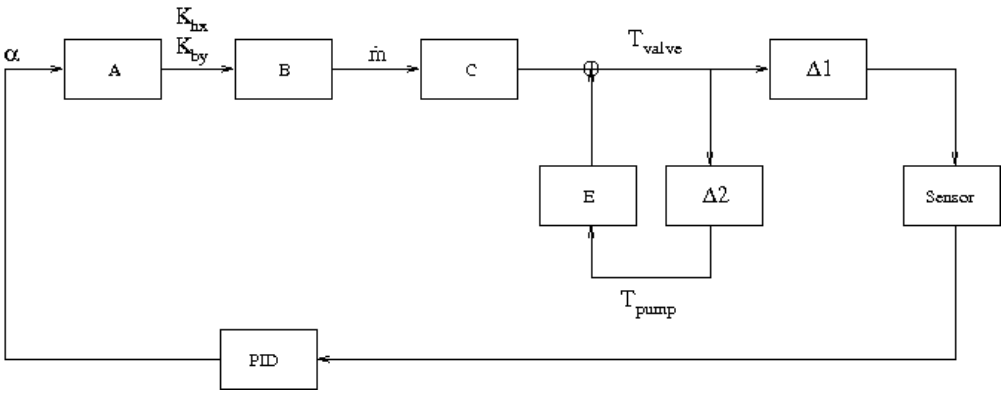

Figure 11 – Plenum Inlet subsystem Transfer Function

AB, PID, Sensor and time delays are the same as for the CHX Inlet side, but with different constants.

Simplified Nyquist Stability Criterion

With the transfer function available, control system stability can be determined. Since the resulting transfer function is too complex to find poles and zeros, Nyquist stability criterion is used. The Nyquist curve of a transfer function G(s) is the curve of G(iω) in the complex plane when ω goes from 0 to infinity. According to the (simplified) Nyquist criterion, the system is unstable if the curve hits or surrounds the point -1. If the curve crosses the real axis to the right of the -1 point, then the system is stable. [10]

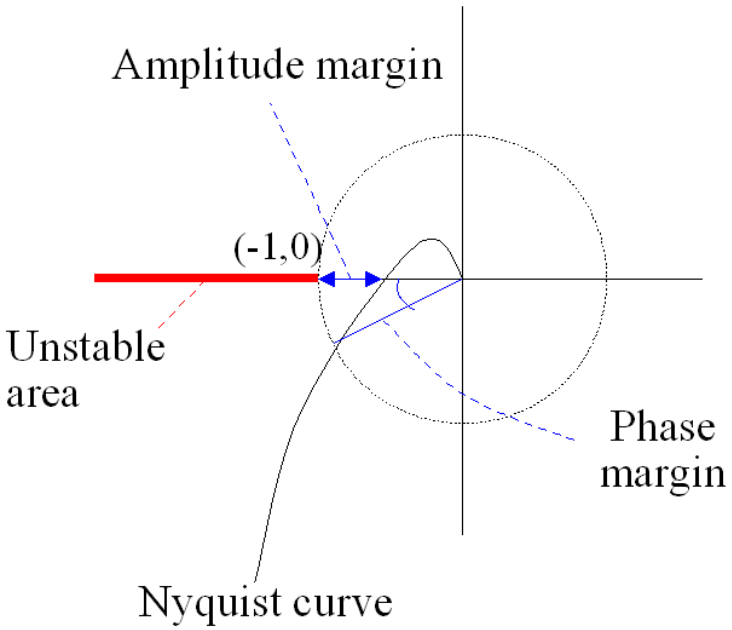

Figure 12 – Nyquist plot and margins

As far as stability margin is concerned, the two traditional stability margins, the amplitude margin and the phase margin, both have problems for the kind of transfer functions involved.

For the amplitude margin, that is the distance between where the Nyquist curve crosses the real axis and the point (-1,0), the problem is that there may be several crossings and it would be difficult to automatically locate the outermost crossing of the Nyquist curve and the real axis (see Figure 13).

For the phase margin, that is the angle between the real axis and where the Nyquist curve crosses the unit circle, the problem is that with a high derivative (D) control constant, the Nyquist curve goes into large circles and in this case the system is not nearly as stable as the phase margin indicates (see Figure 14).

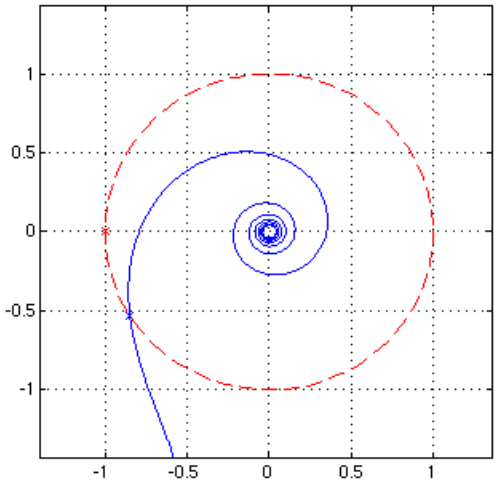

Figure 13 – Example of Nyquist plot where determining the amplitude margin is difficult, because the curve crosses the line from -1 to 0 many times.

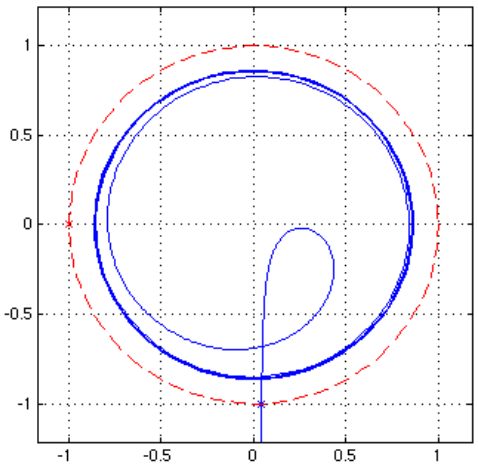

Figure 14 – Example of Nyquist plot when phase margin is not useful. This is from a case with a very large derivative control constant.

Instead, the shortest distance between the Nyquist curve and the point (-1,0) is used to measure stability margin. The value will range from 0 (unstable) to 1 (very stable).

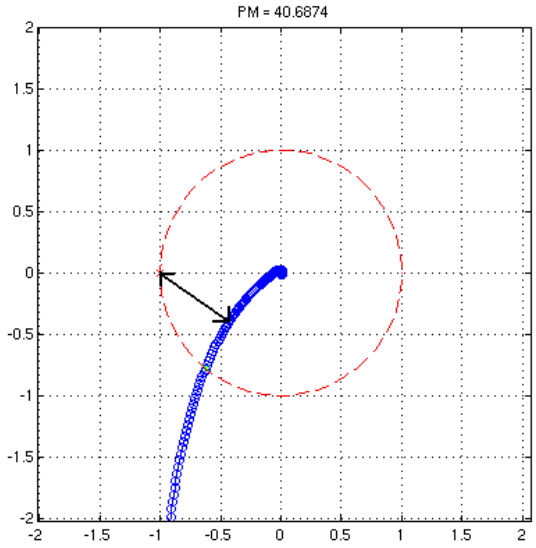

Figure 15 – Vector Margin

Implementation

The calculation of the transfer function and stability margin for a given set of control parameters is implemented in Matlab code. The main difficulty is finding the shortest distance, which is equivalent to minimizing the function abs(1+G(iω)). Minimizing a

function is a common computing problem and the primary issue is finding the global minimum and not a local minimum. This is archived by a heuristic mixing the Nelder-Mead simplex method (Matlab's fminsearch function) and sampling logarithmically equally spaced points, and manually inspecting the Nyquist plot to ensure the closest point is found.

Then, a range of control parameters is swept making a stability map. In a two-dimensional map, the effect of varying two control parameters can be displayed. Since the derivative (D) parameter is currently set to zero in the ATCS, the study is focused on the proportional (P) and integrative (I) parameters.

The stability map is produced for a number of test cases (different working points) and for the CHX and plenum side. The equations are the same for all working points, with different constants.

The chosen test cases are:

- Payload racks flow rate: nominal (four payload racks) / low (no racks)

Temperature set-point at CHX of 5°C or 10°C

Results

CHX INLET SUBSYTEM RESULTS

On next plots (from Figure 16 to Figure 19) are reported stability and margin zones. White is most stable and black is least stable. Current control parameters are marked in blue.

The case most likely to be unstable is low flow rate and high set-point. Preliminary analysis of the effect of payload heat load variation indicated that the major contribution to stability is flow rate. Investigation of the effect of heat load and other variations is left to further work.

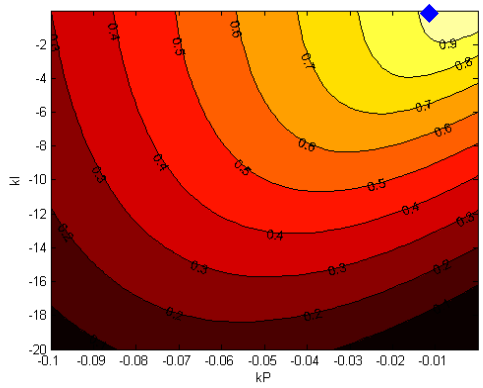

Figure 16 - CHX side, normal flow, set-point 5℃

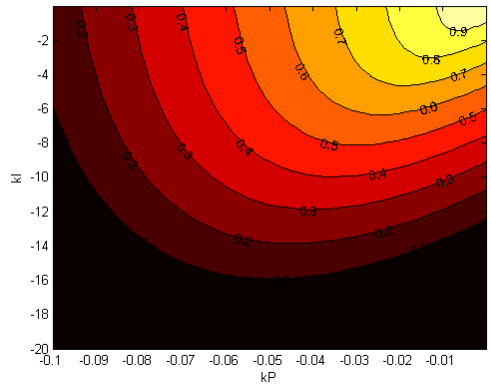

Figure 17 - CHX side, low flow, set-point 5℃

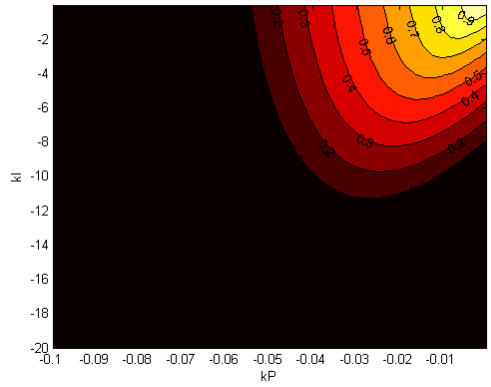

Figure 18 - CHX side, normal flow, set-point 10℃

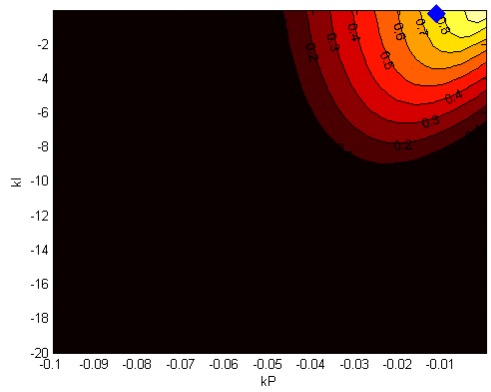

Figure 19 - CHX side, low flow, set-point 10℃

PLENUM INLET SUBSYTEM RESULTS

For the plenum side stability plots are reported here below on Figure 20 and Figure 21. Again the currently used control parameters are marked in blue. The test cases are the nominal flow and chx temperature setpoint 5°C as currently used, and low flow – 10°C at the chx, the case most likely to become unstable.

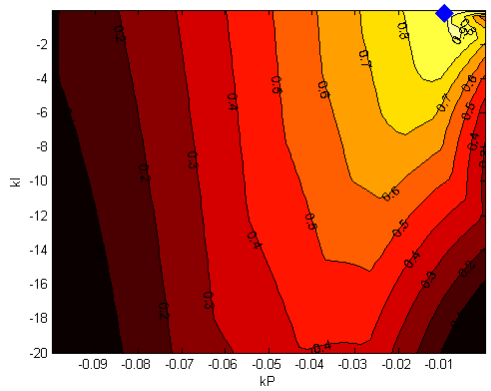

Figure 20 - Plenum side, normal flow, set-point 5℃ in CHX

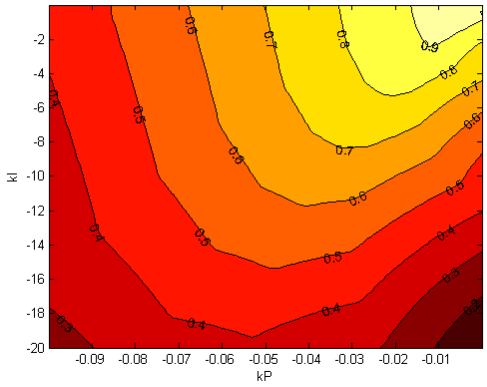

Figure 21 - Plenum side, low flow, set-point 10℃ in CHX

The Nyquist plot for the plenum side with both a short delay between valve and sensor and a long delay through the plenum can be quite complicated. An example near instability is shown in Figure 22.

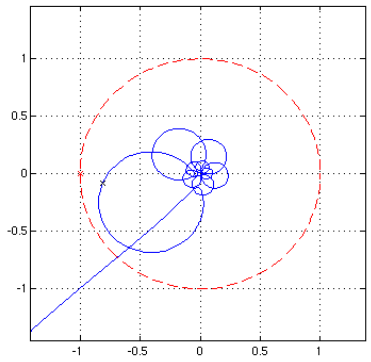

Figure 22 – An example Nyquist plot of the situation near instability on the plenum side.

Verification

Comparison with Simulation

Analytically calculated stability areas are compared with numerical transient simulation using ESATAN/FHTS Thermal Hydraulic Mathematical Model (THMM). The simulated system is let run for a while with the chosen control parameters (see Figure 23). No external disturbance is added. Any instability comes from small deviations that always exist in the system being exaggerated by an unstable control

system. The dead band in the controller is disabled; otherwise small disturbances would have no effect.

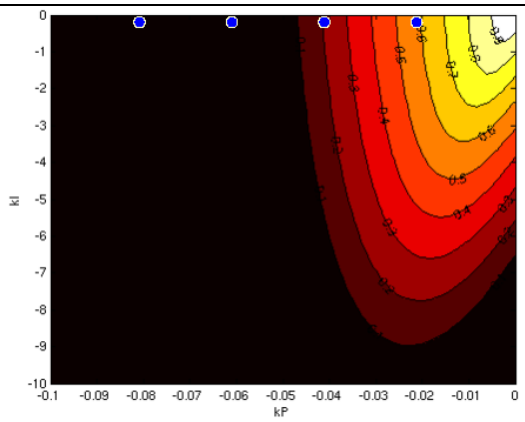

Figure 23 - Control parameters chosen for comparison with ESATAN/FHTS marked with blue dots

The example shown on

Figure **24** of four selected control point on the CHX side is in line with the predictions of the linearized model.

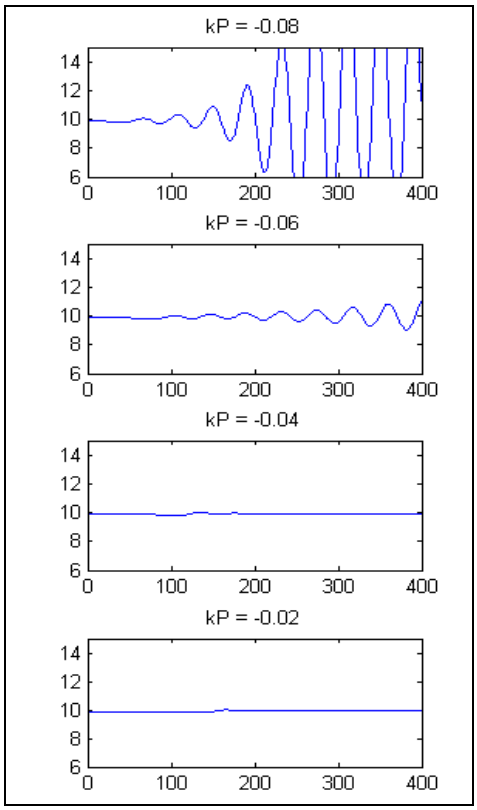

Figure 24 – THMM simulations

Cross Transfer Function

So far, the CHX side ("right") and the plenum side ("left") has been studied separately. To test the validity of this approximation and find possible interactions between the two parts, the effect of disturbances in one side on the other is investigated.

The transfer functions between the two sides can be written down in a similar way as within one side. Specifically, the transfer function from the CHX side to the plenum side describes how a small perturbation in the valve position of WMV 3 or 4 affects the temperature measured at WTSB 1 or 2. The plenum to CHX side transfer function conversely describes the effect of a perturbation of WMV 1 or 2 on WTSB 3 or 4. The other valve is assumed to be fixed in the cross-transfer functions.

$$\begin{cases} G_{\substack{\text{plenum-valve} \\ \rightarrow \\ \text{CHX-sensor}}}(s) = \dfrac{1}{1+\tau_s s} e^{-s\tau_{\text{pipes}}^{(1)}} \left(\dfrac{\dot{m}_{by}^{chx}}{\dot{m}_0^{chx}} e^{-s\tau_{\Delta ISSA}} + \dfrac{\dot{m}_{hx}^{chx}}{\dot{m}_0^{chx}} \dfrac{1-\varepsilon_{LT}}{\frac{M_{LT}}{\dot{m}_{hx}^{chx}} s+1} \dfrac{1-\varepsilon_{MT}}{\frac{M_{MT}}{\dot{m}_{hx}^{chx}} s+1} \right) \dot{m}_0^{chx} \left(\dfrac{d\dot{m}_{hx}^{chx}}{d\alpha_{chx}} \right)_0 \\ \tau_{\text{pipes}}^{(1)} = \dfrac{V_{WMV34 \rightarrow split}}{\dot{m}_0^{plenum}} + \dfrac{V_{split \rightarrow sensor(by)}}{\dot{m}_{by}^{chx}} \end{cases}$$

$$\begin{cases} G_{\substack{\text{CHX-valve} \\ \rightarrow \\ \text{plenum-sensor}}}(s) = \dfrac{1}{1+\tau_s s} e^{-s\tau_{\text{pipes}}} \dfrac{\frac{\dot{m}_{hx}^{plenum}}{\dot{m}_0^{plenum}}}{1-\frac{\dot{m}_{by}^{plenum}}{\dot{m}_0^{plenum}} e^{-s\tau_{around}}} \dot{m}_0^{plenum} \left(\dfrac{d\dot{m}_{hx}^{plenum}}{d\alpha_{plenum}} \right)_0 e^{-s\tau_{\text{pipes}}} \\ \tau_{\text{pipes}}^{(2)} = \dfrac{V_{WMV12 \rightarrow VMV34}}{\dot{m}_0^{chx}} + \dfrac{V_{VMV34 \rightarrow sensor(by)}}{\dot{m}_{by}^{plenum}} \end{cases}$$

The cross-transfer function does not describe a closed loop, so Nyquist stability analysis would be meaningless. Instead Bode plots can be used to study the propagation of disturbances between the two sides at different frequencies.

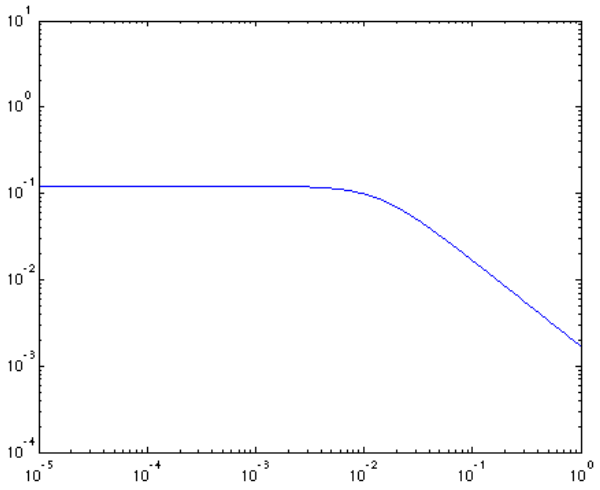

Figure 25 – Bode plot of transfer function from plenum side to CHX side

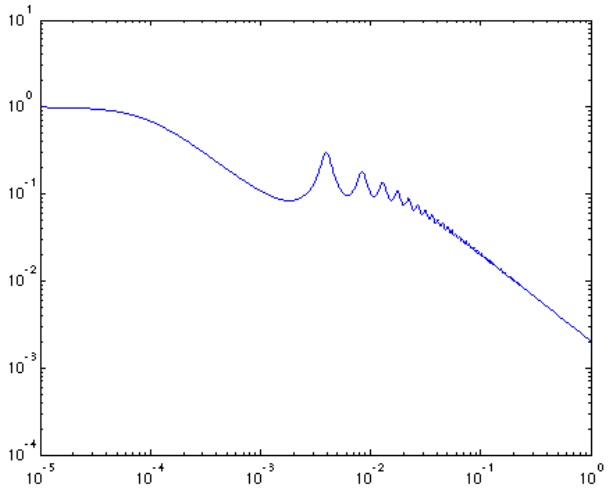

Figure 26 – Bode plot of transfer function from CHX side to plenum side

Interference from the plenum side to the heat exchanger side is damped by the ISS water/ammonia HXs that keep an almost constant temperature. High frequencies are further damped by the sensor.

In the other direction, static changes are completely transferred, but not amplified. There are peaks corresponding to constructive interference between the disturbance itself, and when it comes back after flowing around the plenum, pump and bypass (first peak corresponding to the bypass loop time, 214 s).

Conclusion

The thermal control loop system of the Columbus ATCS have been studied with classical theory and compared with analytical non-linear models.

For the two thermal control loops, it appears that the most important factors determining the thermal control stability is the delay between moving the valve until the temperature change is measured at the sensor. This in turn depends on the water volume between the valve and the sensor and the flow rate. The rise time of the sensor also has some effect.

On the plenum side, there are two time delays: a short delay from the valve (VMV 1 or 2) and the temperature sensors (WTSB 1 or 2), and a longer delay from the valve, through the plenum, pump assembly, bypass piping, through the valve again and to the sensor. Along the longer path, disturbances are damped on the way, but a longer delay in itself is more likely to cause instability.

For both sides and all working points, the current control parameters are well within the stable area. The stability properties predicted using the Nyquist criterion appears to fit well with transient simulations.

Acknowledgements

I wish to thank Jan Person at the Thermal and Environmental Control Section, ESA/ESTEC for advice and guidance throughout my work.

I also wish to thank Professor Claes Breitholtz at Chalmers, the formal examiner of this thesis, for advice and explanations of automatic control theory and for critique of drafts of this report.

Definitions

The following notation is adopted for the “Thermal System Control Analysis”:

- $\dot{m}$ mass flow rate [Kg/h]
- T temperature [°C]
- t, τ time [h]
- P pressure [Pa]

- ♦ K hydraulic resistance [Pa/(kg/h)^2]
- ♦ M water mass [kg]
- ♦ V water volume [m^3]
- ♦ ε heat exchanger efficiency
- ♦ α valve stroke
- ♦ k_P proportional control constant
- ♦ k_I integrative control constant
- ♦ k_D derivative control constant

Acronyms:

ATCS	Active Thermal Control System
CHX	Condensing Heat Exchanger
DB	Dead Band
DMS	Data Management System
DPSB	Delta Pressure Sensor block
ECS	Environmental Control System
EPC	Electronic Package Controller
HX	Heat exchanger
IOTMM	Integrated Overall Thermal Mathematical Model
ISPR	International Standard Payload Rack
LT	Low Temperature
MT	Medium Temperature
PID	Proportional Integrative Derivative (automatic control method)
P/L	Payload
THMM	Thermal Hydraulic Mathematical Model
WMV	Water Modulating Valve
WPA	Water Pump Assembly
WPU	Water Pump Unit

References

1. M. Trichilo, C. Gilardi, S. De Palo "The Columbus Orbital Facility Water Loop Qualification", 1999-01-2001, 29th ICES Conference, July 1999, Denver, Colorado

2. G. Bufano, E. Brach Prever, V. Perotto, P. Vaccaneo, Z. Szigetvari, J. Persson, J. Witt "Columbus Integrated System Level ECS test Correlation", 2004-01-2425, 34th ICES Conference, July 2004, Colorado Spring, Colorado

3. S. De Palo, B. D. Wright, R. W. Clark Jr., B. G. Rhone, Z. Szigetvari, S. Hinderer, J. Persson "Columbus to Human Research Facility Hydraulic Compatibility Test: Analysis and Results", 2005-01-3119, 35th ICES Conference, July 2005, Rome, Italy

4. S. De Palo, P. Vaccaneo "ATCS Re-certification Test. The investigation of Columbus MT Loop Performances Close and Beyond its maximum Operative Limits", 2006-01-2164, 36th ICES Conference, July 2006, Norfolk, Virginia

5. Z. Szigetvari, J. Witt, J. Persson, P. Vaccaneo "Columbus Launch Preparation – Final System ATCS Tests Summary and Lessons Learned", 2008-01-2033, 38th ICES Conference, June–July 2008, San Francisco, California

6. S. De Palo, G. Bufano, P. Vaccaneo, F. Burzagli, M. Bruno, "ATCS Operations During Columbus Mission: Flight Data Evaluation and Correlation", 39th ICES Conference, July 2009, Savannah, Georgia

7. G. Valenzano, F. Burzagli, S. Lombardi, "Temperature Controller Stability resolution for ISS Nodes 2&3 IATCS Loops", 2001-01-2335, 31st ICES Conference, July 2001, Orlando, Florida
8. S. De Paolo "APM ATCS Thermal and Fluidic Analyses and THMM Report", Issue 05, 29 June 2000, Alenia Aerospazio, Document number CLT-RP-AI-0019

9. J. P. Holman “Heat Transfer”, 8th ed., 1997, McGraw-Hill

10. T. Glad, L. Ljung, ”Reglerteknik - Grundläggande teori” (in Swedish), 2:nd ed. Studentlitteratur, 1989

Appendix A: Paper presented at International Conference on Environmental Systems

Presented by Savino De Palo, ThalesAlenia Space, at International Conference On Environmental Systems, July 2009, Savannah, GA, USA, Session: Thermal and Environmental Control Engineering Analysis and Software.

DOI: 10.4271/2009-01-2583

09ICES-0025

Control Stability Analysis Applied to Columbus ATCS

Savino De Palo
ThalesAlenia Space

Tor Klingberg, Jan Persson
ESA-ESTEC

ABSTRACT

Good performance of the Columbus water loop active control system has been demonstrated by several analyses, ground test and is further confirmed by the current flight data. Even so, a comprehensive description of the control within the classical theory is needed, in order to complete the system description, posing also the basis for similar applications to come.
Thermal and hydraulic control loops are considered as two separate systems and linear control methods are applied. Loop stability and performance is discussed by computing stability regions of the PI control coefficients at different loop configurations and results compared with available test, flight and simulation data.

INTRODUCTION

The Columbus laboratory module is the major European contribution to the International Space Station (ISS). It consists of a cylindrical pressurized compartment 4.5 m in diameter and 6.4 m long with room for 10 payload racks. On the outside of Columbus up to 4 attached payloads can be accommodated on a set of consoles. Columbus is designed to offer a shirtsleeve environment for up to 3 crewmembers.

The Columbus thermal control is based on a combination of passive and active techniques. The passive thermal control serves to protect the pressurized compartment from the space environment using multi-layer insulation (MLI) and tuning of the thermo-optical properties of exposed surfaces. The aluminum shell is equipped with heaters with the main purpose to maintain the surface above the maximum dew point temperature of the inside atmosphere in order to avoid condensation.

The objective of the active thermal control is to transport waste heat from subsystems and payloads to interface heat exchangers on Node 2. The coolant medium is water, which is circulated by means of a pump and a grid of water lines and valves to the heat sources and heat sinks. Columbus is allowed to reject a total of up to 22 kW of waste heat to the Medium Temperature (MT) bus heat exchanger and Low Temperature (LT) bus heat exchanger on Node 2, which transfer it from the water to the ammonia in the ISS External Active Thermal Control System (EATCS) and eventually to the radiators on the ISS truss.

The analysis of the operating envelope of the Columbus Active Thermal Control System (ATCS) was validated by tests both at subsystem and system level. The aspect of control was covered by simulations of extreme operating conditions with the validated analysis software code. It has provided empirical verification of the control stability, which has been sufficient in terms of qualification. In a further step, automated control theory is used to explore the ATCS stability margins in order to offer understanding of possible implications on ATCS stability in case changes to ATCS control parameters and of ATCS operation beyond the nominal operating envelope.

ATCS ARCHITECTURE

The ATCS is based on single-loop architecture with the functional requirement to provide adequate cooling capability to

- 10 International Standard Payload Rack (ISPR) locations (4 aftward, 4 forward and 2 overhead)
- 24 cold plate-mounted avionics boxes
- 1 Condensing Heat Exchanger (CHX) with two core elements

A schematic of the layout is included in Figure 1. The MT and LT busses are connected in series to the ATCS. The inlet water to the LT section is a mixture of water from the LT bus, which is at a temperature of 1.1 to 6.1 °C, and warmer water from the WPA, such that the CHX is supplied with water at a constant inlet temperature of 4 to 6.1 °C. The inlet water to the MT section is maintained in the temperature range 16 to 18 °C by mixing of the water from the CHX and water from the LT branch by-pass. The MT section includes the parallel plenum branches for payloads and cold plates

The proper water mixing is commanded to the Water Modulating Valves (WMV) by the WPA software on the basis of Wet Temperature Sensor Block (WTSB) measurements of the CHX and plenum water inlet temperatures. Similarly, the Delta Pressure Sensor Block (DPSB) data form the input to the WPA software on the pressure drop across the plenum and if deviations outside the range 40 to 44 kPa are detected the pump speed is adjusted to return the pressure drop to within the allowable range.

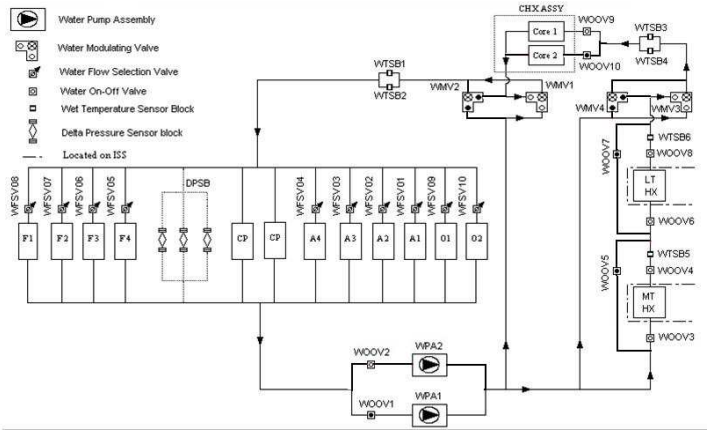

Figure 1 - ATCS schematic

A Water Flow Selection Valve (WFSV) is included upstream of each ISPR permitting regulation of the water flow on the basis of operation timelines. Both the WFSV and the WOOV are designed with a manual override in the form of a hand wheel for the event that commanding via the DMS would not work.

¾" titanium hard lines are used for the main water lines connecting the different parts of the ATCS, while the diameter is reduced to ½" for the ISPR and cold plate branches. ATCS equipment and ISPR connections are done with wire-braid restrained Teflon flex lines in order to achieve the required unit exchange and rack tilting capability.

The ATCS maximum design pressure is 8.34 bar. The WPA maintains the pump inlet pressure at 1.8 bar and with the maximum pump pressure head of 4 bar the pressure in the water loop never exceeds 5.8 bar under normal operating conditions.

The ATCS has a maximum volume of 208 liters, under the assumption that the total ISPR water volume is at the maximum upper limit of 80 liters. An accumulator at the pump inlet has to compensate for thermally induced fluctuations in water volume and the natural level of leakage from the water loop.

ATCS CONTROL

The control algorithms for WMVs and WPA speed are programmed into the WPA Electronic Package Controller (EPC). The EPC hardware is composed of

- 8-bit microcontroller (Intel 80C32)
- PROM bank (2 kB shadow memory for software download)
- RAM bank (8 kB)
- EEPROM (64 kB)
- Watchdog
- Peripherals

The EPC has electrical interfaces to the Data Management System (DMS) through a redundant MIL 1553B data bus and with the 120-VDC Columbus power bus, with the Water Pump Unit (WPU) brushless motor, with the sensors and valves of the accumulator and the filter, with the ATCS sensors and the Emergency, Warning and Caution System (EWACS). The EPC works with a sample frequency of 1 Hz.

Except for water temperature and flow, the EPC software is responsible, as already mentioned, for control of the pump inlet pressure to the applicable set-point, as well as for the acquisition of the WPA sensors and transmission of the sensor data to the DMS.

The control management for water temperature and flow is implemented as closed-control chains operating with a discretized proportional-integrative-derivative (PID) algorithm. For the time $t = t_n$, the control law output is

$$\Delta X = (k_p + \frac{k_i \cdot \Delta t}{2} + \frac{k_d}{\Delta t}) \cdot Err_n +$$
$$+ (\frac{k_i \cdot \Delta t}{2} - k_p - \frac{2 \cdot k_d}{\Delta t}) \cdot Err_{n-1} + \frac{k_d}{\Delta t} \cdot Err_{n-2}$$

where

Err_n = controller input = set-point value – measured value
$= Y_{sp} - Y$
Err_{n-1} = controller input one time step before
Err_{n-2} = controller input two time steps before
k_p = proportional gain
k_i = integrative gain
k_d = derivative gain
Δt = sampling period (1 s)

and the controller output, for time $t = t_n$, can be written $X_n = X_{n-1} + \Delta X$.

The control law performance is influenced by the data acquisition chain (ATCS sensor) accuracy on the input side and the actuator (ATCS component) design on the output side, with the following limitations

- The controller input, *Err*, can assume only discretized values, Err_d, meaning that the acquired input has to be considered to be $Err_d = \mathrm{INT}(Err/\ Y_{min}) \cdot Y_{min}$, where Y_{min} is the minimum difference between the two values of measured variable *Y*
- The controller output variation ΔX has a maximum value $\Delta X \le \Delta X_{max}$
- The controlled parameter X_n has a minimum and a maximum value $X_{min} \le X_n \le X_{max}$
- The controlled parameter X_n can assume only discretized values $X_d = \mathrm{INT}(X/X_{step}) \cdot X_{step}$, where X_{step} is the difference between two consecutive positions of controlled variable

In addition, the control law is not active if the last three error measurements are inside the dead band, DB, i.e. if (($|Err_n|$<DB) and ($|Err_{n-1}|$<DB) and ($|Err_{n-2}|$<DB)) then $\Delta X = 0$. Considering the acquisition chain accuracy, 0.1°C for temperature and 1 mbar for pressure drop, the DB has been set to ±0.3°C for the CHX and plenum inlet temperatures and ±2000 Pa for the plenum pressure drop. It is important to note that DB is adapted so that it is smaller and equal to the specified range for the temperature and flow control.
An additional factor influencing the PID control is the required digitalization of the PID coefficients. Since the PID coefficients are stored as 15-bit binary code words, the approximation due to the binary encoding has to be accounted for.

ATCS MATHEMATICAL MODEL

The simulation of the ATCS water loop is performed with the thermal software tool ESATAN/FHTS. The qualification of the ATCS was based on validation of the modeling approach, in the Thermo-Hydraulic Mathematical Model (THMM), by trimming and correlating the thermo-hydraulic analysis with a large number of test cases which were run on a dedicated test article, reproducing the principal features of the flight version of the ATCS. The testing and analysis validation were part of Water Loop Test Step IV (WLTS IV) in 1998 [1]. From the control standpoint, the major outcome of the WLTS IV was that the worst conditions for the ATCS control system tuning and verification are obtained working with the lowest flow rate, i.e., when no P/Ls are flowed.
Further refinement of the ESATAN/FHTS simulation was performed following the Environmental Control System (ECS) Test on the Columbus PFM in 2003 [2].
The final correlation of the THMM after the ECS Test was judged to be successful since it managed to emulate the same degree of correlation as had been achieved for WLTS IV. Only minor adjustment to the plenum hydraulic resistance was required. The result is shown in next Table 1.
In terms of control stability, it was shown that the temperature and flow control would be able to recover from switching on and off of the coolant flow to a payload with the maximum allowed flow rate of 190 kg/hr. The difference in WPA motor speed between test and analysis results was attributed to difficulties with the calibration of the speed measurement to the actual speed. The speed of the motor in brushless mode is derived from the back-EMF signal, which is conditioned by the WPA EPC before being passed by the I/O interface block to the MIL 1553B data bus

Sensor	Description	Node	Test	THMM
Low flow rate (ECS_010_Step 2)				
WTSB 1	Plenum inlet (°C)	201	17.3	17
WTMO 1	WTMO 1 position (cold flow)	301	42	32
WTSB 3	CHX inlet (°C)	203	5.4	5.4
WTMO 3	WTMO 3 position (cold flow)	303	99	100
DPSB	Plenum pressure drop (mbar)		422	419
	WPA speed (rpm)		5373	5036
	WPA mass flow (kg/hr)		309	308
High flow rate (ECS_070_Step 2)				
WTSB 1	Plenum inlet (°C)	201	17.1	16.6
WTMO 1	WTMO 1 position (cold flow)	301	46	43
WTSB 3	CHX inlet (°C)	203	5.8	5.8
WTMO 3	WTMO 3 position (cold flow)	303	99	100
DPSB	Plenum pressure drop (mbar)		417	415
	WPA speed (rpm)		8991	8374
	WPA mass flow (kg/hr)		687	680

Table 1 - THMM correlation after ECS test

OTHER GROUND TESTS

Beyond [1] and [2], other noteworthy activities at ATCS level was performed on 2004 coupling the system with the Flight Prototype Rack (FPR) of the US payload Human Research Facility (HRF) [3], followed the year after by the Re-certification test campaign [4], which was undertaken to certify the WPA capability to reach an overall flow of 1050 Kg/h. In particular, the former proved an interesting test bed for the hydraulic control performance when coupled with another active control system while the former was used to refine the THMM at highest flow rates.
Final preparation activity was performed at Kennedy Space Center (KSC) just before launch [5]. This test provided data on the WFSV characteristic, useful for fine tuning predictions to be performed with ATCS THMM.

FLIGHT DATA

Columbus was launched with the Space Shuttle Atlantis on February 7th 2008. After activation, the 4 ESA payload racks which had flown to orbit with Columbus were moved from the launch positions and integrated in their designated positions. The payload utilities were connected, one of which is the ATCS, and commissioning was started. Up to February 22nd no payload was operated until the Fluid Science Laboratory (FSL) was started. FSL is located in ISPR location O1 and is calibrated for a flow rate of 170 kg/hr at 40 kPa. The telemetry for the WPA is shown in Figure 2 and Figure 3. Figure 4 shows the corresponding data, applying the in-flight configuration to the correlated THMM.
It is obvious that the IOTMM is able to reproduce, with good fidelity, the on-orbit data. As before, the simulated pump speed is somewhat lower than the measured one, but that is fully in line with the finding during the correlation, as already mentioned.

Since then the ACTS fit flushed several other disturbances, mainly in low flow condition, which is expected to be the worst case scenario. Further, some of these transients were produced by oversized disturbances, like those described in [6], for thermal control and [7] for hydraulic control. Even so, the control system demonstrated to be robust enough to be always stable.

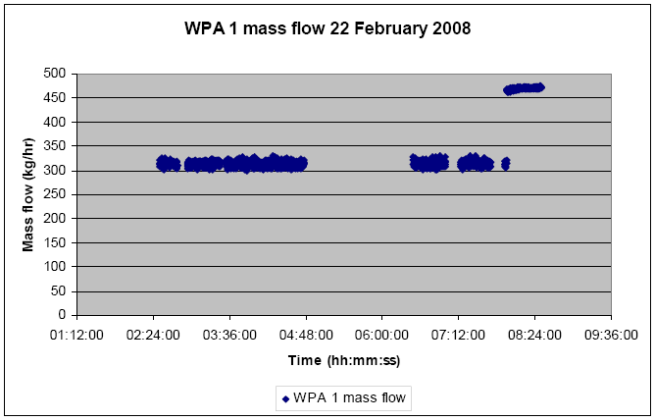

Figure 2 - WPA flow rate, flight data

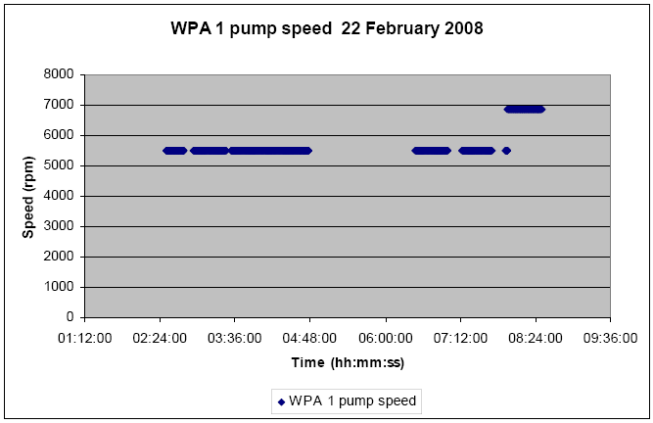

Figure 3 - WPA speed, flight data

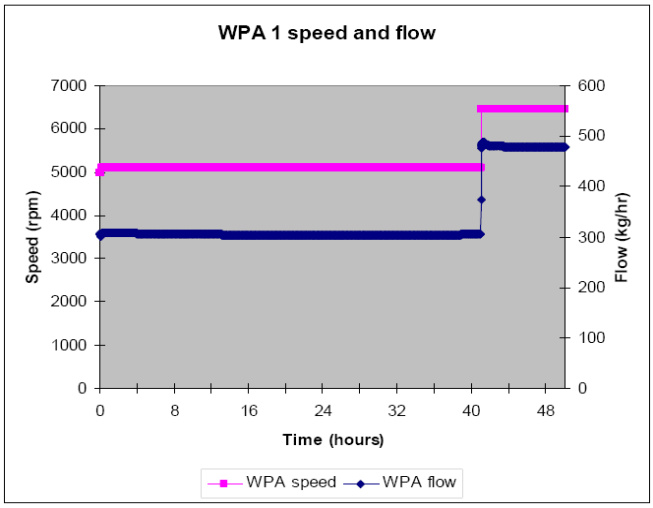

Figure 4 - WPA in-flight simulation

HYDRAULIC SYSTEM CONTROL ANALYSIS

In this paragraph is studied the plenum pressure drop control system. As already mentioned, the system adopts a plenum/distributor configuration: P/Ls and C/Ps are linked in a parallel configuration (the plenum) and mass flow rate control is performed indirectly via the pressure drop at the ends of the plenum. Each branch of the plenum is calibrated, in order to give the required mass flow rate for that plenum pressure drop set-point. Control overcomes disturbances in the loop hydraulic resistance due to movement of valves dedicated to the temperature control, P/Ls opening/closure, WFSVs movements etc..

MATHEMATICAL MODEL

The following assumptions are made to build up a mathematical description of the system:

1. *Pressure drop in the loop zone external to the plenum is constant.*
   This assumption, introduced to simplify calculation, in general is not true: loop pressure drop can change because of movements of valves dedicated to temperature control (e.g., WMVs), reconfiguration of redundant items (e.g., CHX reconfiguration) etc. Analysis results are fully applicable to cases where variation of this hydraulic resistance is due to opening/closure of valves or any other operation that has not closed loop control. It can be also applied in cases where other control loops are present but with higher time constants (as for the temperature control system but no to other hydraulic controls). In these two cases, hydraulic perturbations can be considered as external disturbances to control chain and then does not affect the stability study.

2. *No dynamic term is considered.*
   Hydraulic inertia is negligible if compared to irreversible pressure drop during the fastest hydraulic transient foreseen, acquisition and command frequency of control system. The input/output form of the system is then a simple gain without zero or poles to be included.

3. *Incompressible fluid hypothesis*
   Working fluid is water in a working range where constant density hypothesis can be applied.

4. *Measured pressure drop Δp_{sensor} is equal to pressure drop between the inlet and the outlet of the plenum Δp*
   It is neglected the pressure drop due to piping and other items (connectors, adapters, etc.) connecting the plenum inlet to the DPSB inlet and the DPSB outlet to the plenum outlet. This assumption depends on plenum layout, mass flow rate ranges and plenum pressure drop set point.

5. *Commanded pump speed is equal to the actual pump speed*
   The pump speed control firmware acts almost instantaneously (order of ms) with respect the plenum control system frequency of 1Hz.

In the following, the ATCS hydraulic system is divided into three main elements: the plenum, the pump and the loop (the latter considers the elements not already described in the two previous components). For each element physical equations are provided in non-linear form. The model is then linearized and compared with the equivalent FHTS models results.

Plenum Model

With the above assumptions, the plenum subsystem reduces to the modeling of momentum equation of each branch and mass conservation at the inlet/outlet of the plenum (see Figure 5 below).

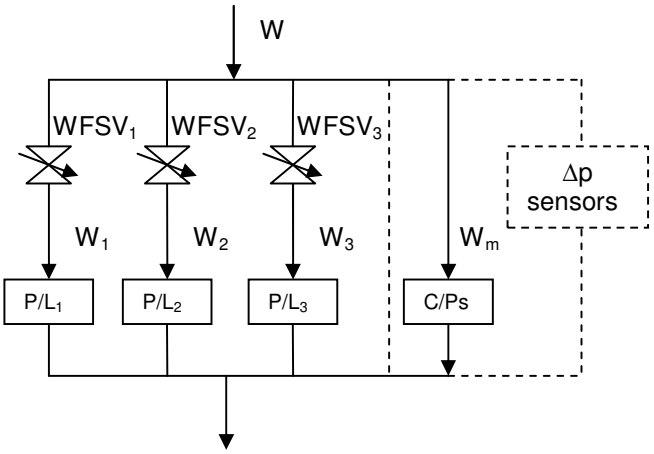

Figure 5 - Plenum Model

Let's denote by W_i the mass flow through branch i of the plenum (with $i=1,2,\ldots,m$) and by r_i the respective hydraulic resistance. If Δp is the plenum pressure drop, for each branch the momentum equation reduces to:

$$\Delta p = r_i \cdot W_i^2 \qquad (i = 1,2,...,m)$$

While the mass (flow) conservation equation is simply:

$$W = \sum_{i=1}^{m} W_i$$

Pump Model:

The centrifugal pump can be described following the Homologous Theory. It is assumed that pump characteristic can be described by a polynomial equation of the second order of the form:

$$f(W,n) = a \cdot n^2 + b \cdot W \cdot n + c \cdot W^2$$

where n is the ration between the working pump speed N and the reference pump speed N_{ref}, and a, b, c are the pump map coefficients calculated for n=1 and W is the pump mass flow rate, which is also the overall plenum flow rate.

Loop Model:

The remaining part of the loop (i.e., excluding plenum and pump) is simply described by its pressure drop coefficient r_o. From hypothesis 1, this resistance is assumed constant and the equation of the loop pressure drop is:

$$\Delta p = f(W,n) - r_o \cdot W^2$$

Non-Linear System Model:

By collecting the above equations, the hydraulic model of the loop system can be written as:

$$\begin{cases} \Delta p = r_i \cdot W_i^2 & (i = 1,...,m) \\ \Delta p = f(W,n) - r_o \cdot W^2 \\ W = \sum_{i=1}^{m} W_i \end{cases}$$

Linearized System Model:

system linearization gives the linear variation δx of a system variable x around its steady state value x^0 due to small variation of the input parameters (for the Hydraulic Analysis all steady state values are indicated with a superscript 0). Without explicating the partial derivative of pump characteristic the system equations set becomes:

$$\begin{cases} \delta(\Delta p) = (W_i^{\,0})^2 \cdot \delta r_i + 2 \cdot r_i^{\,0} \cdot W_i^{\,0} \cdot \delta W_i \qquad (i = 1,...m) \\ \delta(\Delta p) = \left.\dfrac{\partial f}{\partial W}\right|_{n^0, W^0} \cdot \delta W + \left.\dfrac{\partial f}{\partial n}\right|_{n^0, W^0} \cdot \delta n - 2 \cdot r_o \cdot W^0 \cdot \delta W \\ \delta W = \sum_{i=1}^{m} \delta W_i \end{cases}$$

After some algebraic manipulations, the plenum pressure drop variation δ(Δp) can be written as function of normalized pump speed variation δn and the plenum branches perturbation (i.e., P/L opening, P/L closure or P/L recalibration) as follow:

$$\delta(\Delta p) = K \cdot \delta n - \sum_{i=1}^{m} \beta_i \cdot \frac{\delta r_i}{r_i^{\,0}}$$

Where K and β_i are algebraic functions of steady state values n^0, W^0, W_i^0 and r^0. As already mentioned with hypothesis 2, the system model does not contain any dynamic term. As far as control system stability is concerned, only the pump speed term $K\delta n$ must be taken into account.

In order to verify the linearized model, the system gain is also computed numerically with the equivalent FHTS model. For each plenum configuration considered (i.e., different P/Ls mass flow rate calibrations) starting pump speed n^0 is calculated with the control active. Then control is stopped and pump speed is increased/decreased of a fixed value $\delta n^0/2$. Corresponding plenum pressure drop calculated by the code are used in the approximated formula:

$$K = \left.\frac{\delta(\Delta p)}{\delta n}\right|_{n^0} \cong \frac{\Delta p(n^0 + \delta n^0/2) - \Delta p(n^0 - \delta n^0/2)}{\delta n^0}$$

On next Figure 6 are compared the theoretical (linear) model outcomes (continuous line) with sample FHTS (non-linear) model results. The two models provide good agreement between them. This fact gives a good confidence on system gain values obtained.

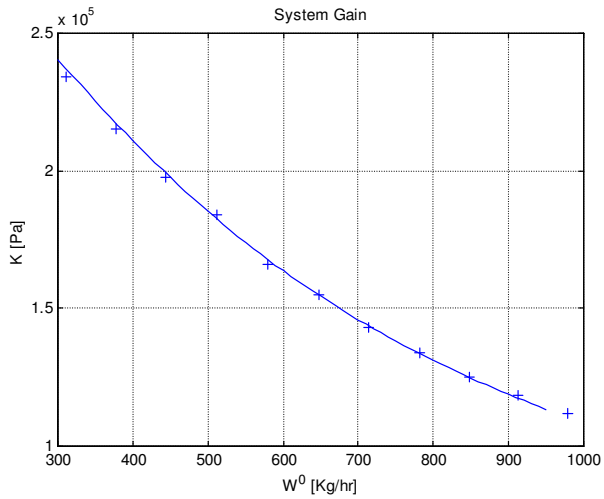

Figure 6 - Gain K vs Loop Mass Flow Rate

The most interesting result is that maximum gain is obtained in the low mass flow rate configuration, i.e., when all P/Ls are closed. From the control perspective the lower is the gain the more stable is the system. In other words, the more P/Ls are open, the more stable is the system. Then worst transient condition for stability check is when only one P/L is open and then its WFSV fully closes, driving the system to its maximum system gain K.

This fact clearly explains some observation performed during WTLS IV [1]. During PID tuning checks, different coefficient sets were tested. Some of them provided some curious behavior like the one reported on next Figure 7 and Figure 8 (time is in seconds), reporting respectively pump speed and plenum pressure drop measurements after P/L simulator valve opening and closure, performed with constant PID coefficients. The close to open perturbation drove the system to lower gain values and vice versa so the control system which was potentially unstable, at the beginning of the first transient recovered its stability because of a reduction of system gain K, but once the second perturbation acted on the system, the original unstable configuration was recovered and oscillations clearly appeared.

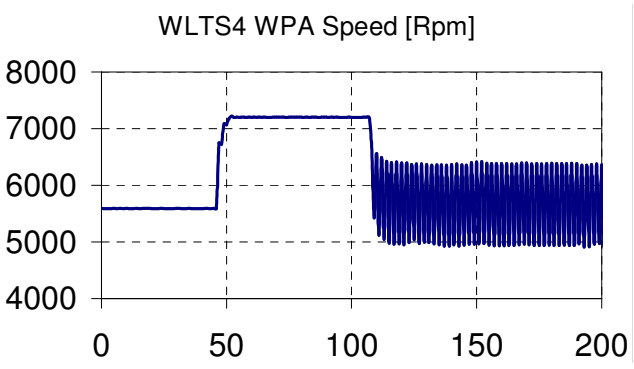

Figure 7 - WLTS IV P/L opening /closure/opening events on Pump Speed

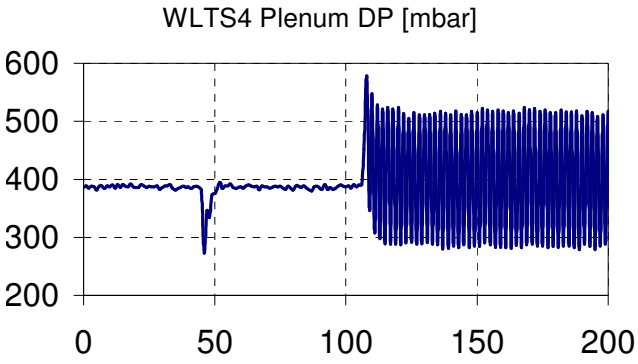

Figure 8 - WLTS IV P/L opening /closure/opening events on plenum ΔP

In Figure 9 the system gain is plotted with external loop hydraulic resistance r_0 reduced/increased by 20% from its nominal value. Lower values of r_0 increases system gain K and then, from system stability point of view, worst case condition is reached for lowest value of r_0. Practically speaking, WMV valves for thermal control system must be fixed into positions that give the lowest value of r_0.

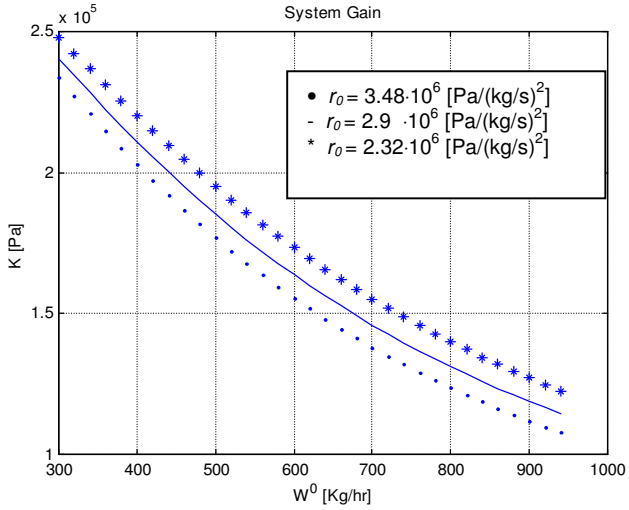

Figure 9 - r_0 Sensitivity on K

CONTROL LAW AND OPEN LOOP TRANSFER FUNCTIONS

Since the time constant in the hydraulic system is negligible, software digitalization must be taken into account. In other words, the time required by the software to acquire inputs, compute and send the command can not be neglected. For this reason the system transfer function must be analyzed in the discrete frequency domain, also known as z or pulse transfer function. This transfer function is the equivalent of the Laplace Transform in the continuous time domain. If $f(t_n)$ is the discrete time function, the z-transfer function F(z) is defined as follow:

$$F(z) \equiv \sum_{k=0}^{\infty} f(t_k) \cdot z^{-k}$$

As for the Laplace Transform, function F(z) can be obtained from f(tn) with simply rules For this analysis is sufficient to know the so called "shifting theorem" which states that:

$$f(tn) \rightarrow F(z) \qquad \Rightarrow \qquad f(tn-m) \rightarrow F(z) \cdot z^{-}$$

As far as the controlled system is concerned, the absence of any time constant gives simply a multiplying constant, i.e.,

$$K(z)=K$$

As far as the controller is concerned, z-transfer function can be obtained directly from PID algorithm equation which gives (for k_d=0):

$$\Delta x(z) = kp \cdot (Err(z) - \frac{Err(z)}{z}) + \frac{ki \cdot T}{2} \cdot (Err(z) + \frac{Err(z)}{z})$$

Where T is the sampling period, equal to 1s. To obtain final value *x(z)* equation must be considered. Its pulse transfer function is:

$$x(z) = \frac{x(z)}{z} + \Delta x(z)$$

After some simple algebraic passages the control system equation becomes

$$y(z) = \left[kp + \frac{ki \cdot T}{2} \cdot \frac{z+1}{z-1} \right] \cdot Err(z)$$

Another important effect that must be taken into account is the command delay. Once the controller has acquired the last error Err and calculated the new output Δx, it gives out the command after a certain time between t_n and t_{n+1}. It does not matter how little this time is: it will be never zero. Even if the (controlled) system reacts instantaneously, the controller will measure this effect only at next time step t_{n+1}. This command delay is represented in the open loop transfer function with an additional term z^{-1}. The complete control scheme is sketched in Figure 10.

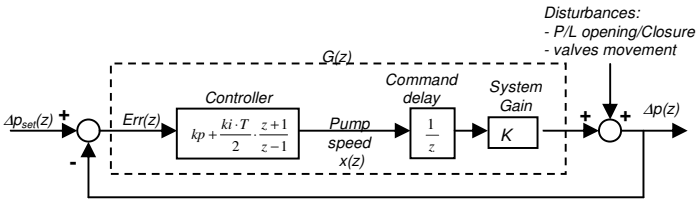

Figure 10 - Hydraulic Control loop scheme

By writing

$$Kp \equiv k_p \cdot K \quad and \quad Ki \equiv k_i \cdot K$$

the final expression for the open loop system transfer function becomes:

$$G(z) \equiv \frac{\Delta p(z)}{Err(z)} = \frac{1}{z} \cdot \left(Kp + \frac{Ki \cdot T}{2} \cdot \frac{z+1}{z-1} \right)$$

and closed loop transfer function is then:

$$\frac{G(z)}{1+G(z)} = \frac{(2 \cdot Kp + Ki \cdot T) \cdot z + (Ki \cdot T - 2 \cdot Kp)}{2 \cdot z^2 + (2 \cdot Kp + Ki \cdot T - 2) \cdot z + Ki \cdot T - 2 \cdot Kp}$$

CONTROL SYSTEM STABILITY ANALYSIS

Once the open-loop pulse-transfer function *G(z)* is known, stability of closed-loop can be determined from the locations of the closed-loop *G(z)/(1+G(z))* poles or, equivalently, from locations of the roots of characteristic equation:

$$P(z)=1+G(z)=0$$

In particular, for the system to be stable, the closed loop poles (or the roots of the characteristic equation) must lie within the unit circle in the z plane. Any closed-loop pole outside the unit circle makes the system unstable.
Closed loop zeros do not affect the absolute stability and therefore may be located anywhere in the z plane.
There are available in the literature different stability tests which can be applied directly to the characteristic equation *P(z)=0* without solving the roots. Here in the following we will apply the Jury stability test, which reveal the existence of any unstable roots, i.e., the roots that lie outside the unit circle in the z plane.

The characteristic equation is a 2nd order polynomial

$$P(z) = a_0 \cdot z^2 + a_1 \cdot z + a_2$$

where

$$\begin{cases} a_0 = 2 \\ a_1 = 2 \cdot Kp + Ki \cdot T - 2 \\ a_2 = Ki \cdot T - 2 \cdot Kp \end{cases}$$

Applying the Jury stability criteria we obtain the following necessary conditions for system stability:

$$\begin{cases} |a_2| < a_0 \\ P(1) > 0 \\ P(-1) > 0 \end{cases} \Rightarrow \begin{cases} |Ki \cdot T - 2 \cdot Kp| < 2 \\ 2 \cdot Ki \cdot T > 0 \\ 4 \cdot (1 - Kp) > 0 \end{cases}$$

These inequalities in the (*Kp , Ki·T*) plane give a triangle shape stability zone which is reported in next Figure 11.

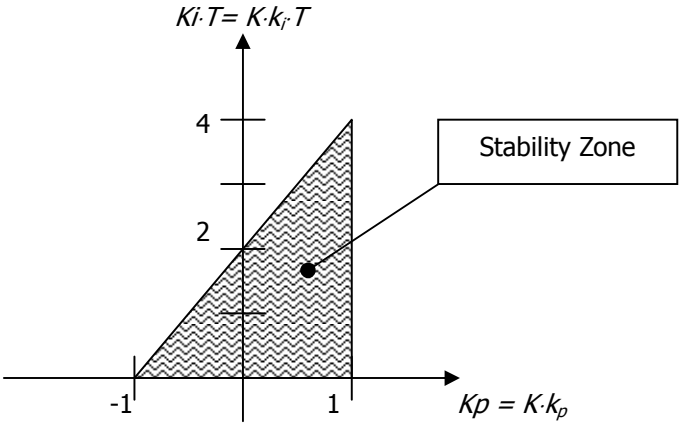

Figure 11 - Stability Zone in the (*Kp,Ki·T*) plane from Jury test

Let's note that stability region in terms of k_p, k_i parameters depends on the system gain *K* and then on the system configuration. In the (k_p , k_i) plane, the stability region has always the same shape but reduces its dimension as the system gain K increases and vice versa. In Figure 12 are reported the stability regions in the (k_p ,k_i) plane for K=2 and K=4.
If (k_p,k_i) set is selected inside the stability region with a low value of K, when K increases the stability region reduces and the (k_p,k_i) point previously selected can lie outside the new stability region. For example, in Figure 12 point (0.35, 1.5) is inside the stability region for K=2 but is outside the stability region for K=4.

Then, in order to have a stable system, the coefficient set (k_p,k_i) to be implemented in the software must be chosen/checked for the highest value of system gain K (the highest value of K must be reached at the end of the transient), which gives the worst condition for the system stability. From this case (highest value of K) stability region can only increase its dimension and then (k_p,k_i) will be always included in the stability zone, giving always a stable system.

Gain K reduces when plenum mass flow rate increases and vice versa. Then, the more P/Ls are open, the more stable is the system, or equivalently, worst transient condition for stability check is when only one P/L is opened and then closes (final condition gives the highest values for K). This behavior was observed with WTLS IV and is also reproduced by FHTS mathematical model.

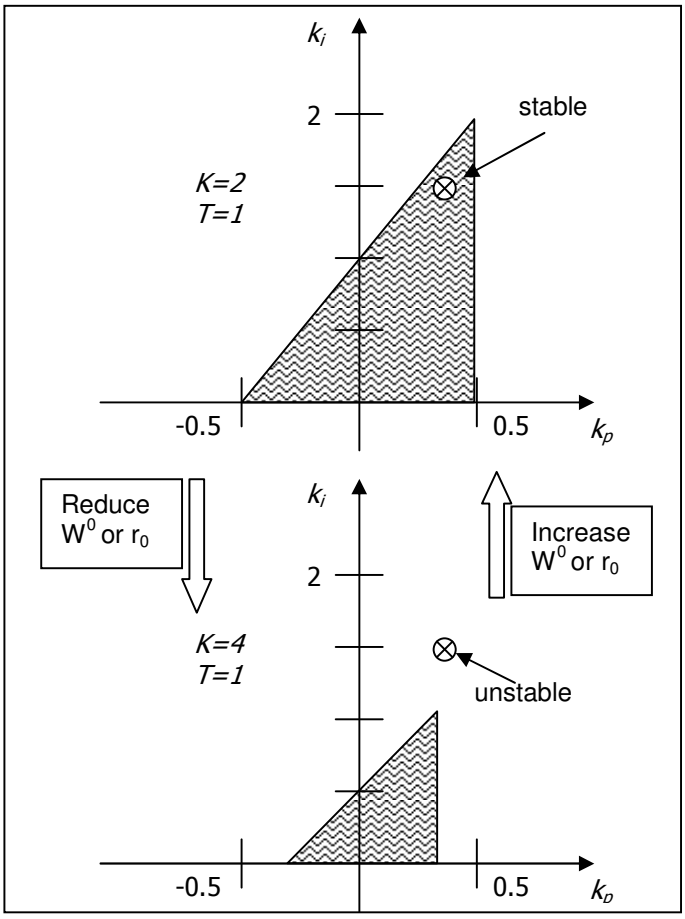

Figure 12 - Stability Zone in the (k_p,k_i) plane with K=2 and K=4

LINEAR VS NON-LINEAR PREDICTIONS

This stability zone is finally checked with ESATAN-FHTS model of Columbus ATCS. System response after P/L closure, with temperature control valves stopped at position α=0.7 and all other P/Ls closed (i.e., low mass flow rate conditions) is checked for different PI coefficients values. These values are reported in Figure 13, with the following legenda:

x = system oscillates

o = system reaches steady state values after some oscillations

+ = system is stable and reaches steady state values without oscillations

First figure gives k_{pN} and k_{iN} stability region. Second figure is stability region in the (Kp,$Ki{\cdot}T$), obtained dividing k_{pN} and k_{iN} by N_{ref} and then multiplying them by current system gain K=2.3643·10^5 [Pa] (this is the gain at the end of the disturbance, i.e., when all P/Ls are closed). Finally Ki is multiplied by acquisition/command time T.

Stability region obtained with Jury criteria is plotted on the same graph: correspondence between FHTS simulations and theory is very good.

Coefficients adopted in flight are k_{pN} = 0.03 [Rpm/Pa] and k_{iN} =0.05 [Rpm/Pa/s]. These values are well enclosed in the stability region for the maximum system gain K=2.3643·10^5 [Pa]: control coefficients adopted in Columbus flight unit ensure a stable and robust control.

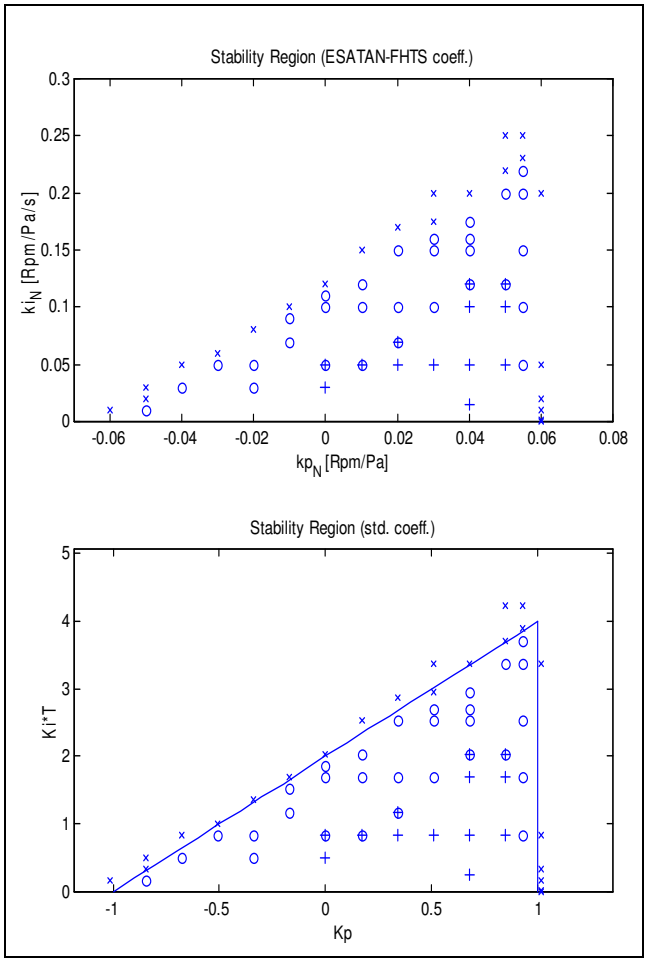

Figure 13 - Stability Region from FHTS vs Jury test

THERMAL SYSTEM CONTROL ANALYSIS

This paragraph focuses on thermal stability analysis. For this study a similar approach adopted for Node 2 and 3 [8] has been adopted.

To make a control theory stability analysis, the system must first be simplified in some ways. First, it is separated into two parts: one for the temperature control for the CHX inlet, and one for the plenum inlet control. The CHX "right" part consists of the water-ammonia heat exchangers (MT and LT), the HX bypass, WMV3&4, WTSB 3&4 and the CHX (see Figure 14). The "left" side

covers WMV1&2, WTSB1&2, the plenum, pumps and cold side bypass (see Figure 15). In the simplified models, the water coming from the other side of the system is assumed to be at a fixed temperature.

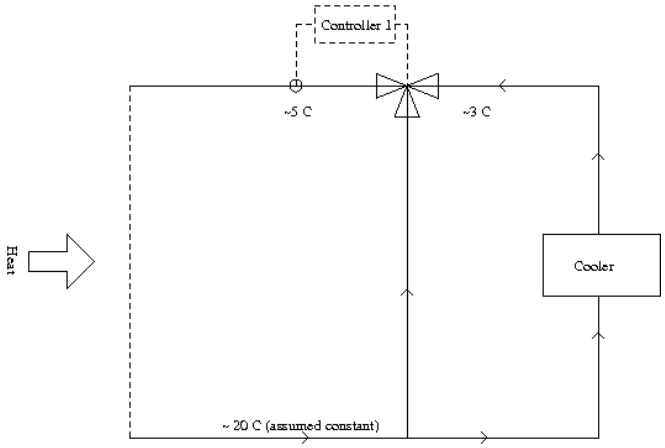

Figure 14 - CHX Inlet subsystem

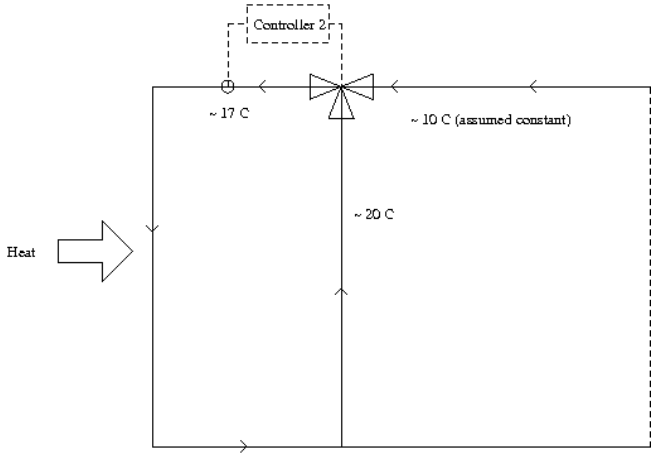

Figure 15 - Plenum inlet subsystem

With the two sides separated, each part is analyzed as a single input-single output (SISO) system, formulating a transfer function description. Specifically, a transfer function that describes how a small change in the system input (signal to the valve control motor) affects the output (temperature measured by the WTSB). That is easiest achieved by combining smaller transfer functions in steps. First, a mathematical model of the system is built, relating valve position, hydraulic resistances, flow rates and temperatures at various places. Each relation is written in the form of a differential equation.

CHX INLET SUBSYSTEM MODEL

CHX inlet subsystem model is composed as follow:

WTSB Sensor

the measured temperature T_s is related to the water temperature at sensor location T_w by:

$$\tau_s \frac{dT_s(t)}{dt} + T_s(t) = T_w(t)$$

The time constant is related to the rise time as

$$\tau_s = \tau_{rise} / 2.2$$

WMV Valve

water temperature at the valve outlet is determined by the mixing of the cold and hot sides, with temperatures T_{LT} and T_0 respectively, i.e.:

$$\dot{m}_0(t) \cdot T_{out}(t) = \dot{m}_{hx}(t) \cdot T_{\mathrm{LT}}(t) + \dot{m}_{by}(t) \cdot T_0(t)$$

With flow rates $\dot{m}_{hx}, \dot{m}_{by}, \dot{m}_0$ depending on the hydraulic resistance of the valve and of the upstream branches.

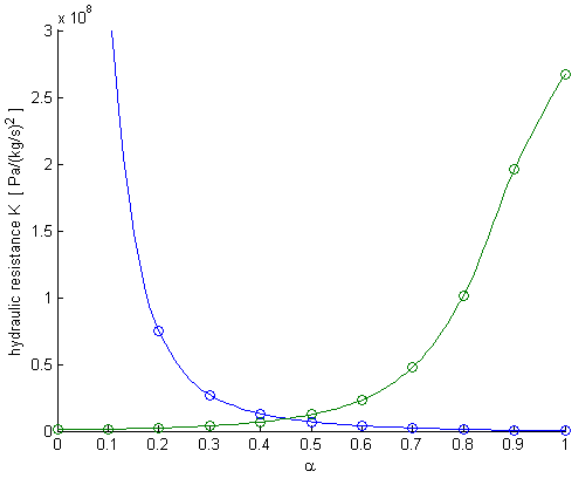

Figure 16 – WMV Hydraulic Resistance vs Position

The hydraulic resistance of the two paths of the valve is interpolated from measured data (Figure 16), while the hydraulic resistances of the two branches are computed directly from the pressure drops in the ESATAN-FHTS simulation at the appropriate working point, with:

$$K = \frac{dP}{\dot{m}^2}$$

Flow rates are then determined by the Bernoulli's law:

$$dP = K \cdot \dot{m}^2$$

imposing equal pressure drop through the HX and bypass sides

$$dP_{hx} = dP_{by}$$

and mass conservation at the valve outlet

$$\dot{m}_{hx} + \dot{m}_{by} = \dot{m}_0$$

Delay Time

delay times for a temperature change to propagate through piping is calculated as

$$\Delta t = V / \dot{m}$$

where V is the sum of the volumes of the piping parts placed between the considered elements.

Heat eXchangers

The effectiveness of the water/ammonia heat exchangers is computed with the classical effectiveness-NTU method [9] for counter flow case:

$$M_{hx}\frac{dT_{hx-out}}{dt} + \dot{m}T_{hx-out} = \varepsilon\dot{m}T_{NH_3} + (1-\varepsilon)\dot{m}T_{hx-\text{in}}$$

Where M_{hx} is the water mass in the heat exchanger and the efficiency factor:

$$\varepsilon = \dot{m}_{NH3}\frac{\left[1-\exp\left(-\frac{UA}{C_{P,H2O}}\left(\frac{1}{\dot{m}_{H2O}}-\frac{C_{P,H2O}}{C_{P,NH3}}\frac{1}{\dot{m}_{NH3}}\right)\right)\right]}{\dot{m}_{NH3}-\frac{C_{P,H2O}}{C_{P,NH3}}\cdot\dot{m}_{H2O}\cdot\exp\left(-\frac{UA}{C_{P,H2O}}\left(\frac{1}{\dot{m}_{H2O}}-\frac{C_{P,H2O}}{C_{P,NH3}}\frac{1}{\dot{m}_{NH3}}\right)\right)}$$

With the overall conductance UA about 7500 W/°K and a constant ammonia flow rate $\dot{m}_{NH3}$ =930 Kg/h and specific heat of $C_{p,H2O}$=4184 J/Kg/°K and $C_{p,NH3}$=4184 J/Kg/°K.

Linearized System Model & Transfer Functions

Some of the differential equations are non-linear, so they must be linearized around a working point, calculated using an ESATAN/FHTS simulation.
The linearized differential equations are then Laplace transformed to form transfer functions. Actually, since the control system operates with a finite frequency of 1 Hz, the Z-transform would be more accurate. However, since thermal fluctuations are slow compared to 1 Hz, the simplification of the continuous Laplace transform is used.

WMV Valve

the relation between hydraulic resistances and flow rate is a quadratic equation that is not easily linearized.

$$\frac{\dot{m}_{hx}}{\dot{m}_0} = -\sigma \pm \sqrt{\sigma^2+\sigma}, \quad \sigma = \frac{K_{by}}{K_{hx}-K_{by}}$$

The sign depends on which gives a physical result $0 \le \frac{\dot{m}_{hx}}{\dot{m}_0} \le 1$ Instead, the values at two valve positions near the working point are compared to calculate the slope.

$$AB(s) = \frac{d\dot{m}_{hx}}{d\alpha} \approx \frac{\dot{m}_{hx}(\alpha^0+\Delta\alpha)-\dot{m}_{hx}(\alpha^0)}{\Delta\alpha}$$

Controller

the transfer function of the controller is

$$\text{PID}(s) = k_P + \frac{k_I}{s} + k_D s$$

In this approximation the dead band, quantization, finite sampling frequency of the controller is ignored.

Heat eXchangers

the flow rate effect on the temperature between the MT and LT heat exchangers is

$$C(s) = \frac{\lambda_{MT}}{M_{MT}s + \dot{m}_{hx}^0}$$

with

$$\lambda_{MT} = (T_{MT}-T_0)\cdot\left(\varepsilon_{MT} + m_{hx}\cdot\frac{d\varepsilon_{MT}}{d\dot{m}_{hx}}\right) + T_0 - T_{hxm}$$

The flow rate effect on the temperature after heat exchangers is

$$F(s) = \frac{\lambda_{\text{LT}}}{M_{\text{LT}}s + \dot{m}_{hx}^0}$$

with

$$\lambda_{\text{LT}} = (T_{\text{LT}}-T_{hxm})\cdot\left(\varepsilon_{\text{LT}} + m_{hx}\cdot\frac{d\varepsilon_{\text{LT}}}{d\dot{m}_{hx}}\right) + T_{hxm} - T_{hxo}$$

Effect of temperature between MT and LT, on the temperature after LT, is:

$$G(s) = \frac{1-\varepsilon_{\text{LT}}}{M_{\text{LT}}/\dot{m}_{hx}^0\cdot s + 1}$$

Direct effect of flow rate on the valve output temperature is

$$I(s) = \frac{T_{hxo}^0 - T_0^0}{\dot{m}_{hx}^0}$$

Effect of HX output temperature on valve output temperature is

$$J(s) = \frac{\dot{m}_{hx}^0}{\dot{m}_0}$$

Delay Time

the transfer function for the time delay τ between WMV outlet and temperature sensor is

$$\Delta_\tau(s) = \mathrm{e}^{-s\cdot\tau}$$

Sensor

the final sensor modeling

$$Sensor(s) = \frac{1}{1+\tau_s \cdot s}$$

The transfer functions for the CHX inlet side are connected as the following diagram:

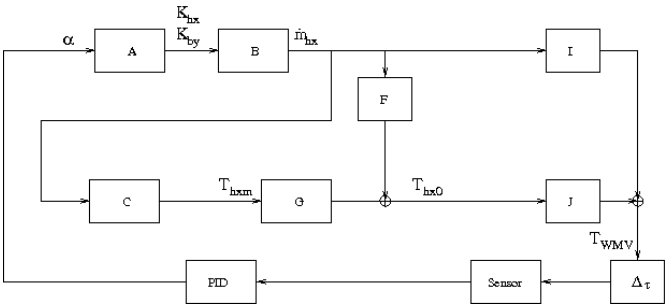

Figure 17 – CHX Inlet subsystem transfer function

By combining transfer functions it can be simplified to:

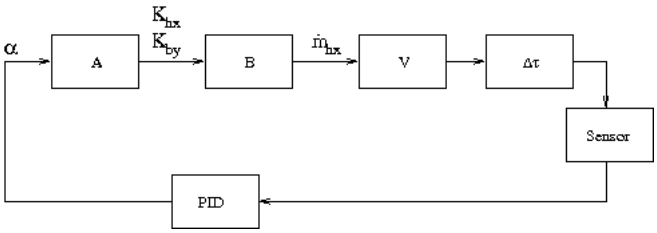

Figure 18 – Simplified CHX inlet subsystem transfer function

With

$$V(s) = I(s) + J(s)\cdot\Delta_{\tau_1}(s)\cdot[F(s) + G(s)\cdot C(s)]$$

PLENUM INLET SUBSYSTEM MODEL

On the plenum side the transfer functions are similar, without the complicated heat exchanger description, but arranged in a different way. One exception is the time for the water to flow through the plenum, pump and back through the cold side bypass to the plenum temperature selection valve. Instead of summing the volumes of all the parts on the way, the time is measured in a transient ESATAN/FHTS simulation by fixing the valve positions, introducing a short heat burst and measuring its travel time. Because of the multiple flow paths through the plenum and the thermal inertia, the heat wave will be smoothed out on the way. The arrival of the first part of the wave is used to measure travel time.

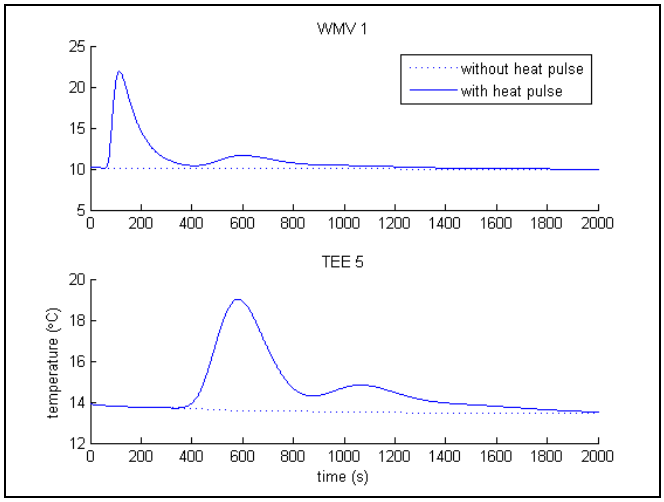

Figure 19 - Heat burst travel time between WMV1 outlet and WMV1 bypass side inlet.

On next Figure 20 is reported the transfer function block of the complete subsystem, with the additional transfer functions C^{plenum} and E^{plenum} which describe the plenum behavior:

$$C^{plenum}(s) = \frac{T_{chx} - T_{pump}}{\dot{m}_{hx}}$$

and

$$E^{plenum}(s) = 1 - \frac{\dot{m}_{hx}}{\dot{m}_0}$$

AB, PID, Sensor and time delays same as for the CHX Inlet side, but with different constants.

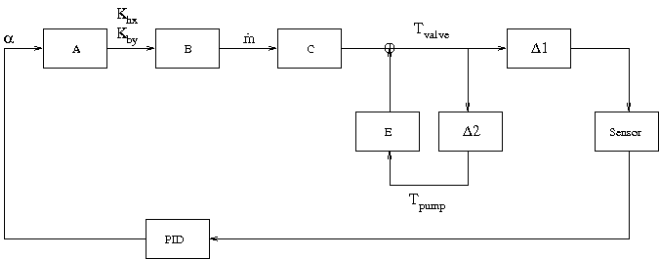

Figure 20 – Plenum Inlet subsystem Transfer Function

NYQUIST STABILITY CRITERION

With the transfer function available, control system stability can be determined. Since the resulting transfer function is too complex to find poles and zeros, Nyquist stability criterion is used. The Nyquist curve of a transfer function G(s) is the curve of G(iω) in the complex plane when ω goes from 0 to infinity. According to the (simplified) Nyquist criterion, the system is unstable if the curve hits or surrounds the point -1. If the curve lies entirely on the right side of the -1 point, then the system is stable.

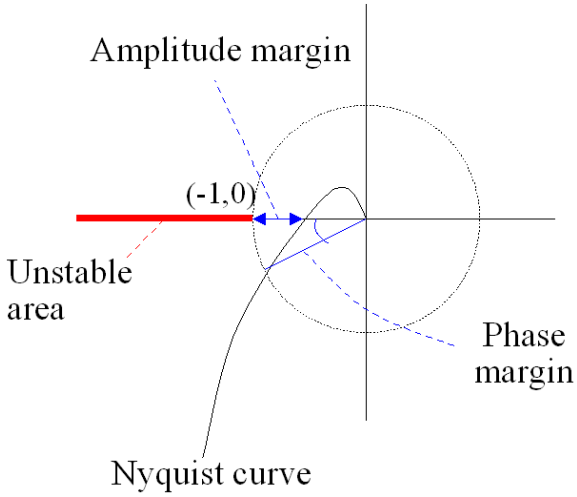

Figure 21 – Nyquist plot and margins

As far as stability margin is concerned, the two traditional stability margins, the amplitude margin and the phase margin, both have problems for the kind of transfer functions involved.
For the amplitude margin, that is the distance between where the Nyquist curve crosses the real axis and the point (-1,0), the problem is that there may be several crossings and it would be difficult to automatically locate the outermost crossing of the Nyquist curve and the real axis (see Figure 22).
For the phase margin, that is the angle between the real axis and where the Nyquist curve crosses the unit circle, the problem is that with a high derivative (D) control constant, the Nyquist curve goes into large circles and in this case the system is not nearly as stable as the phase margin indicates (see Figure 23).

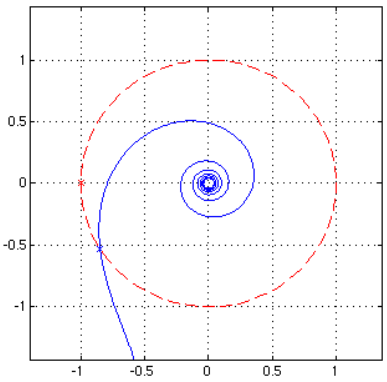

Figure 22 - Example of Nyquist plot where determining the amplitude margin is difficult

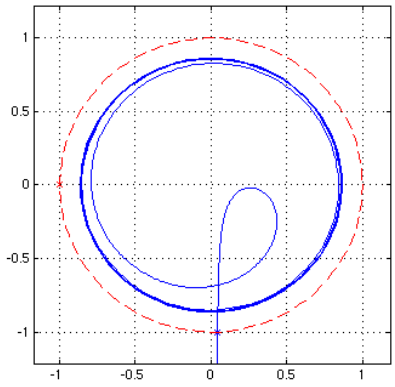

Figure 23 - Example of Nyquist plot where phase margin is not useful

Instead, the shortest distance between the Nyquist curve and the point (-1,0) is used to measure stability margin. The value will range from 0 (unstable) to 1 (very stable).

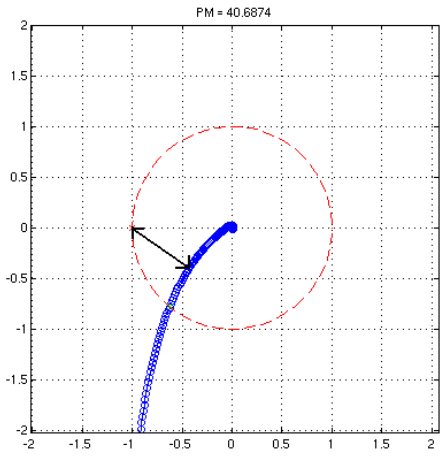

Figure 24 – Vector Margin

The calculation of the stability margin for a given set of control parameters is implemented in Matlab code. The main difficulty is finding the shortest distance, which is equivalent to minimizing the function abs(1+G(iω)). Minimizing a function is a common computing problem and the primary issue is finding the global minimum and not a local minimum. This is archived by a heuristic mixing the Nelder-Mead simplex method (Matlab's fminsearch function) and sampling logarithmically equally spaced points, and manually inspecting the Nyquist plot to ensure the closest point is found.

Then, a range of control parameters is swept making a stability map. In a two-dimensional map, the effect of varying two control parameters can be displayed. Since the derivative (D) parameter is currently set to zero in the ATCS, the study is focused on the proportional (P) and integrative (I) parameters.

The stability map is produced for a number of test cases (different working points) and for the CHX and plenum side. The equations are the same for all working points, with different constants.

The chosen test cases are:

- Payload racks flow rate: nominal (four payload racks) / low (no racks)
- Temperature set-point at CHX of 5°C or 10°C

CHX INLET SUBSYTEM RESULTS

On next plots (from Figure 25 to Figure 28) are reported stability and margin zones. White is most stable and black is least stable. Current control parameters marked in blue.
The case most likely to be unstable is low flow rate and high set-point. Preliminary analysis of the effect of payload heat load variation indicated that the major contribution to stability is flow rate. Investigation of the effect of heat load and other variations is left to further work.

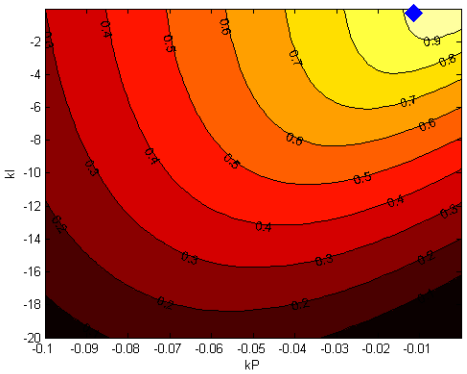

Figure 25 - CHX side, normal flow, set-point 5°C

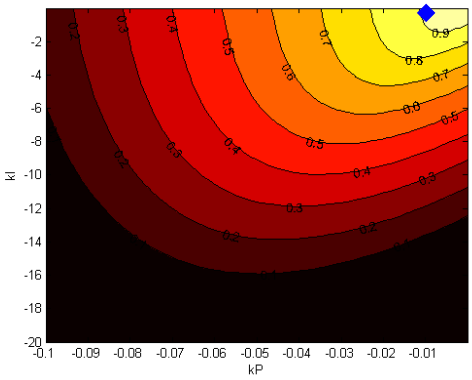

Figure 26 - CHX side, low flow, set-point 5°C

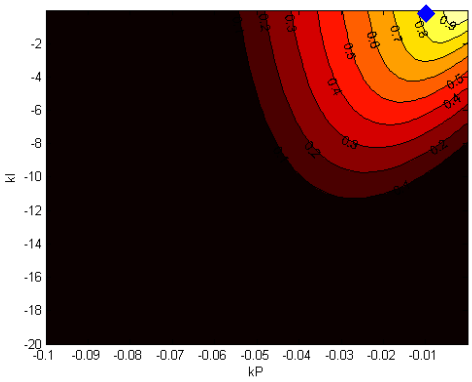

Figure 27 - CHX side, normal flow, set-point 10°C

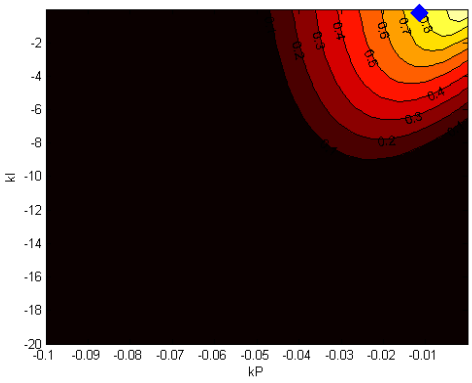

Figure 28 - CHX side, low flow, set-point 10°C

PLENUM INLET SUBSYTEM RESULTS

For the plenum side stability plots are reported here below on Figure 29 and Figure 30. Again the currently used control parameters are marked in blue. The test cases are the nominal flow and chx temperature setpoint 5°C as currently used, and low flow - 10°C at the chx, the case most likely to become unstable.

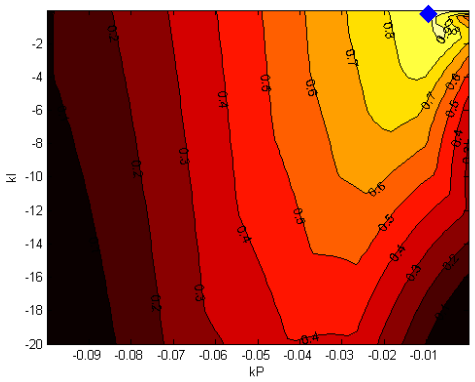

Figure 29 - Plenum side, normal flow, set-point 5°C in CHX

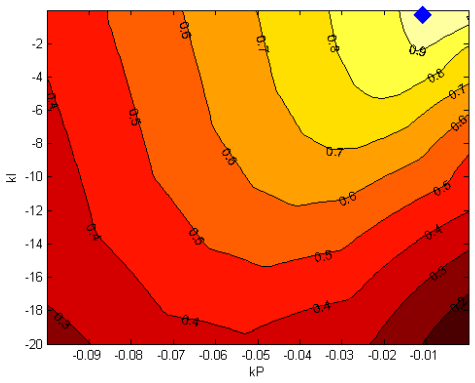

Figure 30 - Plenum side, low flow, set-point 10°C in CHX

The Nyquist plot for the plenum side with both a short delay between valve and sensor and a long delay through the plenum can be quite complicated. An example near instability is shown in Figure 31.

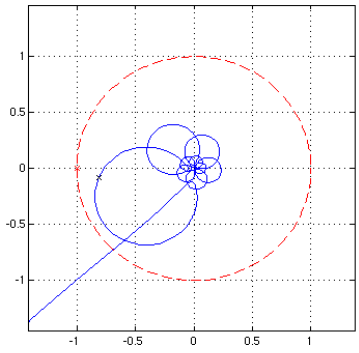

Figure 31 – An example Nyquist plot of the situation near instability on the plenum side.

LINEAR VS NON-LINEAR PREDICTIONS

Analytical calculated stability areas are compared with numerical transient simulation using ESATAN/FHTS THMM. The simulated system is let run for a while with the chosen control parameters (see Figure 32). No external disturbance is added. Any instability comes from small deviations that always exist in the system being exaggerated by an unstable control system. The dead band in the controller is disabled; otherwise small disturbances would have no effect.

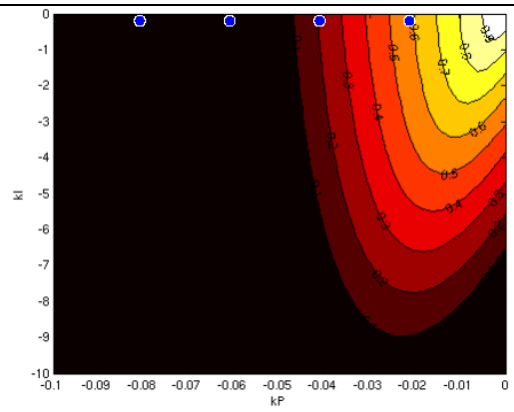

Figure 32 - Control parameters chosen for comparison with ESATAN/FHTS marked with blue dots

The example shown on Figure 33 of four selected control point on the CHX side is in line with the predictions of the linearized model.

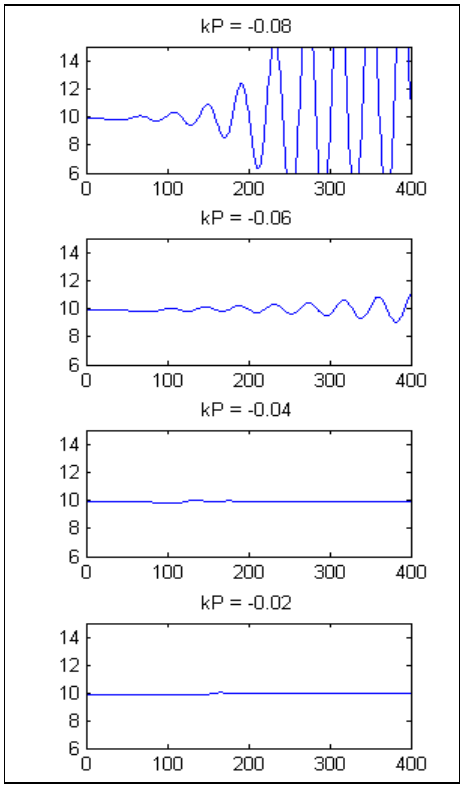

Figure 33 - THMM simulations

CROSS TRANSFER FUNCTION

So far, the CHX side ("right") and the plenum side ("left") has been studied separately. To test the validity of this approximation and find possible interactions between the two parts, the effect of disturbances in one side on the other is investigated.

The transfer functions between the two sides can be written down in a similar way as within one side. Specifically, the transfer function from the CHX side to the plenum side describes how a small perturbation in the valve position of WMV3 or 4 affects the temperature measured at WTSB 1 or 2. The plenum to CHX side transfer function conversely describes the effect of a perturbation of WMV1 or 2 on WTSB3 or 4. The other valve is assumed to be fixed in the cross-transfer functions.

The cross-transfer function does not describe a closed loop, so Nyquist stability analysis would be meaningless. Instead Bode plots can be used to study the propagation of disturbances between the two sides at different frequencies.

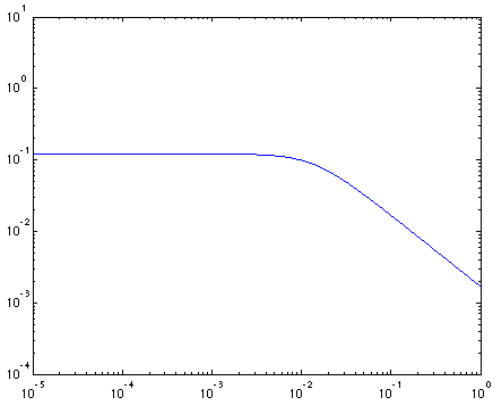

Figure 34 - Bode plot of transfer function from plenum side to CHX side

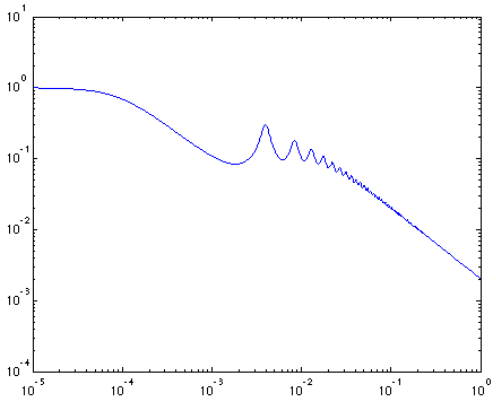

Figure 35 - Bode plot of transfer function from CHX side to plenum side

Interference from the plenum side to the heat exchanger side is damped by the ISS water/ammonia HXs that keep an almost constant temperature. High frequencies are further damped by the sensor.

In the other direction, static changes are completely transferred, but not amplified. There are peaks corresponding to constructive interference between the disturbance itself, and when it comes back after flowing around the plenum, pump and bypass (first peak corresponding to the bypass loop time, 214 s).

CONCLUSION

Both thermal and hydraulic control loop systems of the Columbus ATCS have been studied with classical theory and compared with analytical non-linear models.

As far as hydraulic control is concerned, it is shown that the driving factor is the loop flow rate, with minor influence of the overall hydraulic resistance of the loop: the number and P/Ls connected and their flow calibrations determine the stability margin, lower at low flow rates, i.e., when no P/Ls are connected, while WMV positions have less influence. The current on orbit parameters are well within the stability area also in worst case conditions, as also confirmed by flight telemetry.

For the two thermal control loops, it appears that the most important factors determining the thermal control stability is the delay between moving the valve until the temperature change is measured at the sensor. This in turn depends on the water volume between the valve and the sensor and the flow rate. Once again, the lower the flow rate, the lower is the stability margin. The rise time of the sensor also has some effect.

On the plenum side, there are two time delays: a short delay from the valve (VMV 1 or 2) and the temperature sensors (WTSB 1 or 2), and a longer delay from the valve, through the plenum, pump assembly, bypass piping, through the valve again and to the sensor. Along the longer path, disturbances are damped on the way, but a longer delay in itself is more likely to cause instability.

For both sides and all working points, the current control parameters are well within the stable area. The stability predicted by control theory appears to fit well with transient simulations.

ACKNOWLEDGMENTS

Tor Klingberg wishes to thank Jan Persson at ESA-ESTEC and Claes Breitholtz at Chalmers University of Technology for help and advice.

REFERENCES

1. M. Trichilo, C. Gilardi, S. De Palo "The Columbus Orbital Facility Water Loop Qualification", 1999-01-2001, 29th ICES Conference, July 1999, Denver, Colorado

2. G. Bufano, E. Brach Prever, V. Perotto, P. Vaccaneo, Z. Szigetvari, J. Persson, J. Witt "Columbus Integrated System Level ECS test Correlation", 2004-01-2425, 34th ICES Conference, July 2004, Colorado Spring, Colorado

3. S. De Palo, B. D. Wright, R. W. Clark Jr., B. G. Rhone, Z. Szigetvari, S. Hinderer, J. Persson "Columbus to Human Research Facility Hydraulic Compatibility Test: Analysis and Results", 2005-01-3119, 35th ICES Conference, July 2005, Rome, Italy

4. S. De Palo, P. Vaccaneo "ATCS Re-certification Test. The investigation of Columbus MT Loop Performances Close and Beyond its maximum Operative Limits", 2006-01-2164, 36th ICES Conference, July 2006, Norfolk, Virginia

5. Z. Szigetvari, J. Witt, J. Persson, P. Vaccaneo "Columbus Launch Preparation – Final System ATCS Tests Summary and Lessons Learned", 2008-01-2033, 38th ICES Conference, June-July 2008, San Francisco, California

6. S. De Palo, G. Bufano, P. Vaccaneo, F. Burzagli, M. Bruno, "ATCS Operations During Columbus Mission: Flight Data Evaluation and Correlation", 39th ICES Conference, July 2009, Savannah, Georgia

7. S. De Palo, R. Passini, A. Quaranta, B. D. Wright " Columbus Thermal Hydraulic operations with US Payloads", 39th ICES Conference, July 2009, Savannah, Georgia

8. G. Valenzano, F. Burzagli, S. Lombardi, "Temperature Controller Stability resolution for ISS Nodes 2&3 IATCS Loops", 2001-01-2335, 31st ICES Conference, July 2001, Orlando, Florida

9. J. P. Holman "Heat Transfer", 8th ed., 1997, McGraw-Hill

CONTACT

Savino De Palo, ThalesAlenia Space – Italia
Strada Antica di Collegno, 253 - 10146 Torino, Italy
Phone: +39-011-7180-875
Fax: +39-011-7180-873
e-Mail: savino.depalo@thalesaleniaspace.com

DEFINITIONS, ACRONYMS, ABBREVIATIONS

The following notation is adopted for the "Hydraulic System Control Analysis": all the quantities referring to nominal conditions are superscript with ^{0}, with:

- W mass flow rate [Kg/s]
- N pump speed [Rpm]
- N_{ref} reference pump speed [Rpm]
- n dimensionless pump speed = N/N_{ref}
- Δp plenum pressure drop [Pa]
- r hydraulic resistance [Pa/(kg/s)^2]
- α valve stroke
- S number of steps
- S_{step} total number of steps
- T acquisition/command time step [s]

The following notation is adopted for the "Thermal System Control Analysis":

- $\dot{m}$ mass flow rate [Kg/h]
- T temperature [°C]
- t, τ time [s]
- P pressure [Pa]
- K hydraulic resistance [Pa/(kg/h)^2]
- M water mass [kg]
- ε heat exchanger efficiency
- α valve stroke
- k_P proportional control constant
- k_I integrative control constant
- k_D derivative control constant

Acronyms:

ATCS	Active Thermal Control System
CHX	Condensing Heat Exchanger
DB	Dead Band
DMS	Data Management System
DPSB	Delta Pressure Sensor block
EATCS	External Active Thermal Control System
ECS	Environmental Control System
EPC	Electronic Package Controller
EWACS	Emergency Warning & Caution System
FPR	Flight Prototype Rack
FSL	Fluid Science Laboratory
HRF	Human Research Facility
IOTMM	Integrated Overall Thermal Math. Model
ISPR	International Standard Payload Rack
LT	Low Temperature
MT	Medium Temperature
PFM	Proto Flight Model
PID	Proportional Integrative Derivative
THMM	Thermal Hydraulic Mathematical Model
WLTS	Water Loop Test Step
WMV	Water Modulating Valve
WPA	Water Pump Assy
WPU	Water Pump Unit

Appendix B: MATLAB source code excerpts

```
clear
global ALL

%%%%%%%%%% Load transfer function here %%%%%%%%%%
pTF

%kI = 0.01;
%kP = 1.9;
kD = -0.0000;

%%%%%% Set scan ranges here %%%%%%%
kPL = linspace(-0.015*10/1.5,-0.00001,50);
kIL = linspace(-1*20,-0.00001,50);
%kDL = linspace(-0.0003,0.0005,10);
PM = zeros(length(kPL),length(kIL));
MM=PM;

%%%%%% Show Nyquist plot of this point (figure 1) %%%%%%%%%%
show_kPi = 7;
show_kIi = 15;
%show_kDi = 5;

for kPi = 1:length(kPL)
  kPi
  kP = kPL(kPi);
  for kIi = 1:length(kIL)
  %for kIi = 1:length(kIL)
    kI = kIL(kIi);
    PID = @(x) kP + kD*x + kI./x;
    L = @(x) PID(x) .* ALL(x);
    OnePlusL = @(x) abs(1+L(i*x));


    wmin = fzero( @(w) abs(L(i*w))-1 , 1e-3);
    if(wmin<0)
      wmin = fzero( @(w) abs(L(i*w))-1 , -wmin);
    end
    if(wmin<0)
      disp('Negative wmin');
      wmin
    end
    amin = OnePlusL(wmin);
    wmin2tmp = fminsearch(OnePlusL, 1);
    %wlist = logspace(log10(wmin2tmp)-1,log10(wmin2tmp)+1,1000);
    wlist = logspace(log10(wmin2tmp)-1,log10(wmin2tmp)+2,10000);
    OPLwlist = OnePlusL(wlist);
    [tmpamin,iwmin2] = min(OPLwlist);
    wmin2 = fminsearch(OnePlusL, wlist(iwmin2));
    amin2 = OnePlusL(wmin2);
    wlist2 = linspace(wmin2*0.1, wmin2*2,1000);
    Lwlist = L(i*wlist2);
    if sum( (imag(Lwlist)>=0) & (real(Lwlist)<=-1) )>0
      amin2 = 0;
    end
    if amin2<amin
      amin = amin2;
      %disp('amin2<amin');
    end
```

```
if abs(L(i*1e5)) > 1
  amin = 0;
end
for wloop = logspace(1, 4,100)
  Lloop = L(i*wloop);
  if imag(Lloop) >= 0
    if real(Lloop) <= -1
      amin2 = 0;
    end
    break
  end
end
PM(kPi,kIi) = 2*asin(amin/2) / pi * 180;
MM(kPi,kIi) = amin2;

Lnear = L(i*wmin);
Lnear2 = L(i*wmin2);
if imag(Lnear)>0
  PM(kPi,kIi)=0;
end

if(kPi == show_kPi && kIi == show_kIi)
  kP
  kI
  wmin2
  boolList = (imag(Lwlist)>=0) & (real(Lwlist)<=-1)
  if sum( (imag(Lwlist)>=0) & (real(Lwlist)<=-1) )>0
    disp 'Foop!'
  end
  for wloop = logspace(2, 3,1000)
    Lloop = L(i*wloop);
    if imag(Lloop) >= 0
      wloop
      Lloop
      if real(Lloop) <= -1
        amin2 = 0;
      end
      break
    end
  end
  wmin
  logwmin = log10(wmin)
  %hf = abs(L(i*1e5))
  %lf = abs(L(i*wmin/100))
  %w = logspace(logwmin-2, logwmin+2,1000);
  w = logspace(-1, 4,10000);
  %w = linspace(0,10,1000);
  Ldata = L(i*w);
  figure(1)
  clf
  plot(real(Ldata), imag(Ldata),'-')
  axis([-5 5 -5 5])
  axis square
  grid on
  hold on
  plot(-1,0,'xr')

  plot(real(L(i*wmin)), imag(L(i*wmin)),'ok')
  plot(real(L(i*wmin2tmp)), imag(L(i*wmin2tmp)),'dk')
```

```
      plot(real(Lnear2), imag(Lnear2),'xk')
      %title(['PM = ' num2str(PM(kPi,kIi))]);
      %draw unit circle
      angle = linspace(0, 2*pi);
      y=sin(angle);
      x=cos(angle);
      plot(x,y,'r--')
      %Laround = L(i*1/(dtvp+dts)*2*pi);
      %plot(real(Laround), imag(Laround), 'kd')
      shg
      %pause
    end
  end
end

[kIM, kPM] = meshgrid(kIL, kPL);
%%%%%% Phase margin %%%%%%
% figure(2)
% clf
% [c,h] = contourf(kPM, kIM, PM);
% colormap hot
% clabel(c,h)
% xlabel kP
% ylabel kI
% hold on
% plot(kPL(show_kPi), kIL(show_kIi), 'bo')


%%%%%% distance from (-1,0) stability margin %%%%%%%%%%%
figure(3)
clf
[c,h] = contourf(kPM, kIM, MM);
colormap hot
clabel(c,h)
xlabel kP
ylabel kI
hold on
%plot(kPL(show_kPi), kIL(show_kIi), 'bo')
caxis([0 1])
```

Published with MATLAB® 7.7

```
global ALL

%%%%%%%% Define transfer functions and parameters here %%%%%%%%%%

%Parameters
m_hx = 143.481332;  % from ESATAN simulation [Kg/h]
m_by = 834.952045;  %ESATAN [Kg/h]
m0 = m_hx + m_by;   % [Kg/h]


Psplit = 397743.619; %ESATAN [Pa]
Phx = 387784.5;    %ESATAN [Pa]
Pby = 396858.351;    %ESATAN [Pa]
dPhx = Psplit - Phx;  %[Pa]
dPby = Psplit - Pby;  %[Pa]
Khx = dPhx/m_hx^2;    %[Pa/(Kg/h)^2]
Kby = dPby/m_by^2;    %[Pa/(Kg/h)^2]

Tchx = 11.5918503; %ESATAN    [C]
Tpump = 18.2323418; %ESATAN    [C]
tau_rise = 25/3600; %Sensor spec  [h]
mvs = 1.1279; %Mass from valve to sensor  [kg]

tau_s = tau_rise/2.2; % [h]
dts = mvs/m0;         % [h]
dm = m_hx*0.01;
% dtvp = 214/3600;       % [h] Pulse travel measure *0.1
dtvp = 81/3600;       % [h] Pulse travel measure *0.1

alpha0 = 0.198354668;  %ESATAN [Dimensionless in range 0-1]
alpha1 = alpha0 + 0.01;
if alpha1>1
  disp('alpha1 too large!');
end
v_alpha = 0:0.1:1;
WMV1_HX = [9.959954613 8.523337271 7.874436048 7.432168728 7.114621156
    6.841785571 6.601814932 6.365720998 6.126776973 5.821352369 5.716008396];
WMV1_BY = [5.950241127 6.169067246 6.361084079 6.589223860 6.832204270
    7.090285690 7.364998395 7.680290261 8.005202872 8.291501605 8.426529536];
KhxWMV0 = interp1(v_alpha, WMV1_HX, alpha0, 'cubic');
KhxWMV1 = interp1(v_alpha, WMV1_HX, alpha1, 'cubic');
KbyWMV0 = interp1(v_alpha, WMV1_BY, alpha0, 'cubic');
KbyWMV1 = interp1(v_alpha, WMV1_BY, alpha1, 'cubic');
Khx0 = Khx + 10^KhxWMV0/3600^2;
Khx1 = Khx + 10^KhxWMV1/3600^2;
Kby0 = Kby + 10^KbyWMV0/3600^2;
Kby1 = Kby + 10^KbyWMV1/3600^2;
sigma0 = Kby0/(Khx0-Kby0);
sigma1 = Kby1/(Khx1-Kby1);
mm0 = -sigma0 + sqrt(sigma0^2+sigma0);
if mm0<0 || mm0>1
  mm0 = -sigma0 - sqrt(sigma0^2+sigma0);
end
if mm0<0 || mm0>1
  disp 'No good mmm0 found!';
end

mm1 = -sigma1 + sqrt(sigma1^2+sigma1);
```

```
if mm1<0 || mm1>1
  mm1 = -sigma1 - sqrt(sigma1^2+sigma1);
end
if mm1<0 || mm1>1
  disp 'No good mmm1 found!';
end
d_mm_d_alpha = (mm1-mm0)/(alpha1-alpha0);


% Transfer functions
TF_A = @(s) 1;
TF_B = @(s) m0*d_mm_d_alpha;
TF_C = @(s) (Tchx - Tpump)./ m_hx;
TF_D = @(s) m_hx ./ m0;
TF_E = @(s) 1 - m_hx ./ m0;


plenum_time_constant = 50/3600*1; % >0 adds a slowness in the plenum
TF_valve_pump = @(s) exp(-s*dtvp) .* 1./(1+plenum_time_constant*s);;
TF_Deltas = @(s) exp(-s*dts);
TF_G_sensor = @(s) 1./(1+tau_s*s);

% Bundled TFs
TF_Q = @(s) (TF_C(s) .* TF_B(s) .* TF_A(s)) ./ (1 - TF_E(s) .* TF_valve_pump(s));
TF_R = @(s) TF_D(s) ./ (1 - TF_E(s) .* TF_valve_pump(s));
TF_S = @(s) TF_E(s) ./ (1 - TF_E(s) .* TF_valve_pump(s));

ALL = @(s) TF_G_sensor(s) .* TF_Deltas(s) .* TF_Q(s);
```

Published with MATLAB® 7.7